Gut regulates brain synaptic assembly through neuroendocrine signaling pathway

Yanjun Shi [1], Lu Qin [1], Zhiyong Shao [1*]

1. Department of Neurosurgery, State Key Laboratory of Medical Neurobiology and MOE Frontiers Center for Brain Science, Institutes of Brain Science, Zhongshan Hospital, Fudan University, Shanghai 200032, China.

*Corresponding author and lead contact

Electronic address: shaozy@fudan.edu.cn.

Abstract

The gut-brain axis plays an essential role in regulating neural development in response to external environmental stimuli, such as microbes or nutrient availability. Defects in gut-brain communication usually lead to various neurological disorders. However, it remains unknown whether gut plays any intrinsic role in regulating neuronal development. Through a genetic screen in *C. elegans*, we uncovered that an intrinsic Wnt-endocrine pathway in gut regulates synaptic development and neuronal activity in brain. Specifically, the gut expressed neuropeptide NLP-40 upregulated by a canonical Wnt signaling, which then facilitates presynaptic assembly through regulating GPCR AEX-2 mediated neuronal spontaneous activity. Therefore, this study not only uncovers a novel synaptic development mechanism, but also reveals a novel gut-brain interaction.

Key words: Gut-brain axis; Synaptic development; Wnt; CWN-2; Endocrine; Neuropeptide/NLP-40; GPCR/AEX-2

The gastrointestinal (GI) tract plays a critical role in regulating brain development and function. It not only provides the nutrient, but also senses the external environmental stimuli. The gut-brain communication is recognized as gut-brain axis. Through this axis, diets and gut microbes can regulate neurogenesis, microglia and astrocyte activation, myelination, blood brain barrier permeability, synaptic pruning and plasticity (Cryan et al., 2019). Dysregulation in the gut-brain axis is correlated with various neurodevelopmental or neurodegenerative disorders (Mulak and Bonaz, 2015; Li and Zhou, 2016; Quigley, 2017; Kowalski and Mulak, 2019; Chidambaram et al., 2020). Although accumulative evidence indicates that gut signaling affects neuronal development and function in the brain, it remains largely unknown if it plays any intrinsic role in brain development.

Gut-brain communication is mainly mediated through three pathways: afferent nervous system, immune system and endocrine system (Wang and Wang, 2016). Among those, the endocrine system is the most complex and highly conserved in both vertebrates and invertebrates (Bernhard Kleine and Rossmanith; Dimaline and Dockray, 1994; Campbell et al., 2004; Nassel et al., 2019). Upon stimulating by nutrients or gut microbiota, enteroendocrine cells (EECs) release neuropeptides or hormones such as cholecystokinin (CCK), ghrelin, leptin, peptide tyrosine-tyrosine (PYY), and glucagon-like peptide-1 (GLP-1) which can travel a long distance as endocrine factors through binding GPCR or other type of receptors to regulate the feeding behavior and the physiological function of the nervous system (Dockray, 2013; Wang et al., 2013). However, it is largely undetermined whether the intestinal endocrine system is involved in neurodevelopment or synaptic formation.

In this study, we uncovered that a canonical Wnt pathway, which is a conserved development programming signaling, acts in the intestine to regulate synaptic development in the nerve ring, which is the nematode's brain.

We further demonstrated that the Wnt signaling functions through upregulating the neuroendocrine molecule NLP-40, which then promotes the synaptic assembly through the neuronal receptor AEX-2/GPCR. Therefore, our study reveals a novel gut-brain interaction underlying synaptogenesis in brain.

Results

Intestinal Wnt signaling regulates AIY presynaptic formation

C. elegans AIY neurons are a pair of bilateral symmetric interneurons located in the head (Fig. 1A) (White et al., 1986). AIY neurites form presynapses onto their target neurons in the nerve ring with a stereotypic and highly reproducible pattern (Fig. 1A') (Colon-Ramos et al., 2007; Shao et al., 2013). We previously found that the canonical Wnt signaling is required for normal AIY presynaptic morphology, and the ligand CWN-2 and the receptor CFZ-2 act both cell-autonomously in the AIY and non-cell-autonomously in the intestine (Shi et al., 2018). To address if the Wnt signaling pathway regulates the AIY presynaptic formation, we first quantified the fluorescent intensity of the AIY synaptic vesicle marker GFP::RAB-3 and active zone marker GFP::SYD-1 in the loss-of-function mutants *cwn-2(ok895)*, *cfz-2(ok1201), pop-1(hu9)* and *sys-1* RNAi animals. We found that loss of this Wnt signaling resulted in a robust reduction of both synaptic markers (Fig. 1B-H, 1B'-H'). To exclude the possibility that the reduction of the presynaptic marker was specific to the GFP fluorophore, we quantified the mCherry::RAB-3 and obtained similar results (Supplementary Fig. 1A-G). These results collectively suggest that canonical Wnt signaling is required for AIY presynaptic assembly.

To determine the site of action for the Wnt signaling, we knocked down the Wnt receptor and the downstream signaling components through neural or intestinal specific RNAi. Interestingly, we found robust reduction of the presynaptic markers after knocking down Wnt signaling in the intestine (Fig.

1I-N), but not in the nervous system (Fig. 1I'-N'). Consistently, the *cfz-2(ok1201)* mutants could only be rescued by the intestine-specific, but not by the neuronal-specific, expression of *cfz-2* cDNA (Supplementary Fig. 2D-F). These data collectively suggest that CWN-2 acts through canonical Wnt components CFZ-2/SYS-1/POP-1 in the gut to regulate AIY presynaptic formation in the brain.

Intestinal neuropeptide/NLP-40 is required for synaptogenesis

The gut can communicate with the brain through the neuroendocrine signaling pathway(Dimaline and Dockray, 1994; Campbell et al., 2004; Nassel et al., 2019). To test whether Wnt signaling in the gut acts through neuropeptide signaling, we first examined if EGL-3, a key proprotein convertase (PC2) involved in neuropeptide maturation (Li and Kim, 2008), was required for the AIY presynaptic assembly. Indeed, the fluorescence intensity of AIY presynaptic markers was robustly reduced in *egl-3(n589)* mutants ($P<0.01$, Fig. 2A), suggesting that neuropeptides are required for the AIY presynaptic assembly. 115 neuropeptide encoding genes have been identified in *C. elegans* genome (Nathoo et al., 2001; Li and Kim, 2008). We screened most neuropeptide genes enriched in the intestine through RNAi for AIY synaptic regulators (Fig. 2B) (Pauli et al., 2006; Li and Kim, 2008; Spencer et al., 2011; Wang et al., 2013). Interestingly, *nlp-40* displayed a dramatic reduction of AIY presynaptic marker, suggesting that it is required for the synaptic assembly (Fig. 2C).

To confirm if AIY synaptogenesis requires *nlp-40*, we first examined the AIY synaptic phenotype in two independently isolated *nlp-40* mutant alleles, *tm4085* and *vj3* (Wang et al., 2013). *nlp-40(tm4085)* harbors an in-frame deletion that delete P1 and part of P2, A70 to V mutation in the P3 and an early stop deleting the last three amino acid at the C-terminus of P4 (Fig. 2D and

Supplementary Fig. 3). The *vj3* deletes the *nlp-40* promoter, the first exon and first intron (Fig. 2D)(Wang et al., 2013). Similar to the RNAi results, we observed a robust reduction of the AIY synaptic vesicle marker GFP::RAB-3 in both *nlp-40* mutant alleles (Fig. 2E-G, J). Similar results occurred with the active zone marker GFP::SYD-1 (Supplementary Fig. 4A-D, A'-C'). The AIY presynaptic defects in *nlp-40(tm4085)* and *nlp-40(vj3)* mutants were rescued by the wild type *nlp-40* transgene (Fig. 2H-J). Interestingly, overexpressing *nlp-40* in wild-type animals does not affect the AIY GFP::RAB-3 fluorescent intensity, suggesting that the role of *nlp-40* in AIY presynaptic assembly is not simply dosage-dependent (Supplementary Fig. 5A-C). Based on these data, we conclude that *nlp-40* is required for AIY synaptogenesis.

Next, we wanted to determine the NLP-40 action site. First we examined the *nlp-40* expression pattern with both transcription and translational reporters and found *nlp-40* was detected in the intestine beginning at early embryonic stages, and the protein was observed both in the intestine and the coelomocytes which is consistent with previous report (Supplementary Fig. 6A-E) (Wang et al., 2013). Then, using intestinal specific RNAi to knock down *nlp-40*, we observed a robust reduction of AIY presynaptic marker GFP::RAB-3, phenocopying the *nlp-40* mutants (the GFP::RAB-3 was reduced by 54.48%. $P < 0.01$; Fig. 2K-M). These data collectively suggest that *nlp-40* is expressed in the intestine and secreted to pseudocoelom. Therefore, the intestinal expressed NLP-40 most likely travels to the nervous system and promotes AIY presynaptic assembly.

To address when *nlp-40* is required for the AIY presynaptic formation, we quantified the fluorescent intensity of AIY GFP::RAB-3 in *nlp-40(tm4085)* mutants at the larval L1, L4 and adult day 1 stage. We found the GFP intensity was dramatically reduced in the *nlp-40(tm4085)* mutants as of the newly hatched L1 stage throughout the adult stage (Supplementary Fig. 6F-H, 6F'-H',

6I). These data suggest that intestinal *nlp-40* is required for AIY presynaptic assembly during embryonic development.

nlp-40 **acts downstream of the Wnt signaling pathway to promote AIY presynaptic assembly**

Thus far, we demonstrated that AIY presynaptic assembly requires both Wnt signaling and *nlp-40* from the intestine. To determine the nature of their interaction, we examined the genetic interaction between the genes encoding Wnt signaling components and *nlp-40* by building three sets of double mutants: *cwn-2(ok895);nlp-40(tm4085), cfz-2(ok1201);nlp-40(tm4085)* and *pop-1(hu9);nlp-40(tm4085)*. We found that the fluorescent intensity of the AIY presynaptic marker GFP::RAB-3 in all double mutants was similar to that in *nlp-40(tm4085)* single mutants, but slightly weaker than in Wnts single mutants (Fig. 3A). The epistatic effects of *nlp-40* to Wnt genes suggest that *nlp-40* acts downstream of the Wnt signaling pathway to regulate AIY presynaptic assembly.

The above genetic data prompted us to test whether the Wnt signaling pathway regulates *nlp-40* expression. First, we quantified the *nlp-40* mRNA levels by quantitative reverse transcription PCR, and found that *nlp-40* mRNA levels were significantly reduced in *cwn-2(ok895), cfz-2(ok1201),* or *pop-1(hu9)* mutants compared to wild-type animals (Fig. 3B). Then, we quantified the *nlp-40* transcriptional reporter P*nlp-40::*GFP and observed a significant reduction of the GFP intensity in *cwn-2(ok895), cfz-2(ok1201)* or *pop-1(hu9)* mutants or *sys-1* RNAi animals (Fig. 3C-I). To exclude the possibility that Wnt signaling affects the overall expression of intestinal genes, we examined the expression of intestinal specific *erm-1* and *vha-6* reporters. Both reporters were not affected by genetic mutations or RNAi knockdown of the same set of Wnt signaling components (Fig. 3J-P and Supplementary Fig. 7A-F). Together,

our data demonstrate that the Wnt signaling pathway upregulates the expression of NLP-40, which then promotes AIY presynaptic assembly.

The peptide P3 derived from NLP-40 is required for the AIY presynaptic assembly

nlp-40 encodes a neuropeptide precursor protein, which contains a N-terminal signal peptide sequence and four predicted mature peptides (P1 to P4 in Fig. 4A) (Wang et al., 2013). To test which of the four peptides regulates the AIY presynaptic assembly, we constructed four NLP-40 mutant variants (M1 to M4), each containing three mutant sites inactivating one corresponding mature peptide (Fig. 4A) (Wang et al., 2013). While the M1, M2 and M4 partially or fully rescued the AIY synaptic defect in *nlp-40(tm4085)* mutants, the M3 was not able to rescue at all (Fig. 4B-H, 4I). Those data indicate that the P3 is required for the AIY presynaptic assembly.

The NLP-40 GPCR receptor AEX-2 acts cell-autonomously in the AIY to regulate presynaptic assembly

AEX-2 serves as the NLP-40 receptor to regulate rhythmic behavior or anoxic survival (Wang et al., 2013; Doshi et al., 2019). To test whether *aex-2* regulates AIY presynaptic assembly, we examined the fluorescent intensity of the presynaptic marker in *aex-2(sa3)* mutants and found a dramatic reduction in AIY GFP::RAB-3 intensity (Fig. 5B, H). Furthermore, we found that the reduction of the AIY presynaptic intensity in *aex-2(sa3)* mutants was rescued by a wild-type *aex-2* transgene (Fig. 5E, I). The data suggest that *aex-2* is required for AIY presynaptic formation.

To test the genetic interaction between *nlp-40* and *aex-2*, we quantified the AIY presynaptic marker GFP::RAB-3 in the *nlp-40(tm4085);aex-2(sa3)* double mutants. We found that the GFP intensity in the double mutants was similar to

that in either single mutants (Fig. 5B-D, H), indicating that *nlp-40* and *aex-2* act in the same genetic signaling pathway to regulate AIY presynaptic assembly. The genetic interaction data is consistent with the model that AEX-2 acts as the NLP-40 receptor to regulate the AIY presynaptic assembly.

Next, we wanted to determine the *aex-2* action site. First, we built an *aex-2* transcription reporter, which showed that *aex-2* was mainly expressed in the nervous system with some in the posterior intestine (Fig. 5J). When colabeled with the AIY cytoplasmic marker P*ttx-3::mCherry*, we noted that the *aex-2* reporter was co-labeled with the AIY reporter (Fig. 5K-K''), indicating that *aex-2* is expressed in AIY interneurons. To address where *aex-2* acts, we expressed *aex-2* cDNA with AIY- or intestine-specific promoter in the *aex-2(sa3)* mutants, and found that only AIY-specific expression rescued the presynaptic defect (Fig. 5F, G, I). These data suggest that *aex-2* acts cell-autonomously in the AIY interneurons to regulate presynaptic formation.

The Wnt-endocrine signaling regulates AIY activity.

The mature neuropeptide/NLP-40 activates GABAergic neurons (Wang et al., 2013; Oliva and Inestrosa, 2015). To determine if Wnt/*nlp-40/aex-2* regulates AIY activity, we recorded the AIY calcium activity using GCaMP6, a genetically encoded calcium indicator (Fig. 6A and 6A') (Luo et al., 2014). In wildtype animals, the AIY automatically fires about six times. However, in *cfz-2(ok1201)*, *nlp-40(tm4085)* or *aex-2(sa3)* mutants, it only fires three times (Fig. 6B-C, Movie S1). The fire amplitude was not affected (Fig. 6D). These data suggest that Wnt/*nlp-40/aex-2* signaling pathway promotes AIY synaptic assembly probably through regulating AIY activity.

The Wnt/*nlp-40*/aex-2 signaling pathway is required for the presynaptic assembly in the nerve ring

We have shown that the canonical Wnt signaling in the intestine promotes the presynaptic assembly of AIY interneurons in the nerve ring mediated by the neuropeptide NLP-40. To determine if the Wnt/NLP-40/AEX-2 signaling pathway is generally required for presynaptic assembly in the nerve ring, we first quantified the intensity of the pan-neuronal synaptic marker GFP::RAB-3 in the nerve ring region. Interestingly, the synaptic marker GFP::RAB-3 was significantly reduced in *cwn-2(ok895)*, *cfz-2(ok1201)* and *pop-1(hu9)* mutants (Fig. 7A-E, H), suggesting that the Wnt signaling is required for the presynaptic assembly throughout the nerve ring.

Next, we tested whether presynaptic assembly in the nerve ring requires *nlp-40* and *aex-2.* We quantified the nerve ring GFP::RAB-3 intensity in *nlp-40(tm4085)* and *aex-2(sa3)* mutants. Similar to that found in Wnt mutants, the GFP intensity was also significantly reduced (Fig. 7F, G and H), indicating that *nlp-40* and *aex-2* are also required for presynaptic assembly in nerve ring.

To confirm the role of Wnt/NLP-40/AEX-2 pathway in regulating presynaptic assembly in the nerve ring, we tested whether the presynaptic defect of the nerve ring in the mutants could be rescued by the corresponding wild-type transgenes. Indeed, we found that the reduction of the synaptic GFP::RAB-3 in nerve ring in *cwn-2(ok895), nlp-40(tm4085)* and *aex-2(sa3)* mutants were rescued by the corresponding transgenes (Fig. 7I) . These data collectively demonstrate that the pro-synaptogenic role of Wnt/NLP-40/AEX-2 signaling pathway is not specific to AIY, but general for most neurons in the nerve ring region.

Discussion

Overall, we demonstrate that a canonical Wnt signaling pathway that includes Wnt/CWN-2, Frizzled/CFZ-2, β-catenin/SYS-1 and TCF/POP-1 acts in the intestine to promote synaptic assembly in the *C. elegans* nerve ring, a

structure analogous to mammalian brain. Wnt signaling exerts this effect by upregulating the expression of *nlp-40*, which encodes a conserved neuropeptide. NLP-40 promotes synaptic assembly through the neuronal expressed GPCR receptor, AEX-2. We uncover a previously unidentified molecular mechanism in which the Wnt-neuroendocrine signaling pathway in the intestine regulates synaptic assembly. These results highlight the intrinsic role of gut in the neurodevelopment, and reveal a novel function of novel gut-brain communication.

Wnt-Neuropeptide axis regulates synaptic assembly

The genes encoding Wnt signaling pathway components and their roles in synaptogenesis are highly conserved (Park and Shen, 2012; He et al., 2018). However, the underlying mechanisms are not completely understood. In this study, we uncovered a novel molecular mechanism underlying Wnt regulating synaptic assembly. In this pathway, the canonical Wnt signaling promotes synaptic assembly by upregulating the expression of the intestinal secreted neuropeptide, NLP-40, which acts through the neuronal expressed GPCR, AEX-2.

Wnt ligands can act either in the nervous system or in non-neuronal tissues to regulate synaptic assembly or plasticity. However, the receptors or downstream components only acted in neurons or their target cells. For example, the Wnt ligands, LIN-44 and EGL-20, expressed in the tail suppress presynaptic assembly through the frizzled receptor LIN-17 or MIG-1 in DA8, DA9 and DB7 neurons (Klassen and Shen, 2007; Mizumoto and Shen, 2013). Presynaptic CWN-2 and LIN-44 regulate activity-dependent postsynaptic localization of the acetylcholine receptor ACR-16 mediated by the LIN-17 and CAM-1 receptors in the postsynaptic muscle cells (Jensen et al., 2012; Pandey et al., 2017). Through β-catenin and TCF/LEF transcription factors, the

canonical Wnt signaling regulates the abundance of glutamate receptor GLR-1 in the postsynaptic neurons (Dreier et al., 2005). Here, we found that a canonical Wnt signaling in the intestinal cells, but not the neurons, promotes synaptic assembly in the *C. elegans* brain through the neuropeptide-like peptide NLP-40.

NLP-40 belongs to the neuropeptide-like proteins (NLPs) family and is required for rhythmic defecation and anoxia survival (Husson et al., 2005; Wang et al., 2013; Doshi et al., 2019). Neuropeptides are small bioactive signal peptides including insulin-like peptides (INS), FMRFamide-related peptides (FLPs) and neuropeptide-like proteins (NLPs) (Li and Kim, 2008). Those peptides are expressed both in the nervous system and non-neuronal tissues with a broad spectrum of biological functions (Li and Kim, 2008; Hu et al., 2011; Hu et al., 2015; Chew et al., 2018). For example, INSs regulate aversive learning behavior (Lee and Mylonakis, 2017) and feeding state-dependent gene expression in ADL neurons (Gruner et al., 2016). FLPs modulate the locomotion and body wave and head search behaviors (Reinitz et al., 2000; Davis and Stretton, 2001; Li, 2005; Chikka et al., 2016). Similarly, NLPs regulate locomotion, body posture, rhythmic behaviors (Couillault et al., 2004). However, the role of neuropeptides in neuronal development or synaptic assembly was largely underdetermined previously.

The role of Wnt in synaptic development is highly conserved in vertebrates (Budnik and Salinas, 2011; Park and Shen, 2012; He et al., 2018). For example, Wnt7a and Wnt5a play critical roles in pre- or postsynaptic development in mammals (He et al., 2018). Although the role of Wnt-neuropeptide in synaptic development was previously not reported, The Wnt/β-catenin has been shown to regulate the expression of gut hormone/neuropeptides (Garcia-Martinez et al., 2009; Garcia-Jimenez, 2010; Kim et al., 2015), suggesting that Wnt-neuropeptide interactions are

evolutionally conserved. In addition, hormones/neuropeptides are also involved in synaptic assembly and function in mammals (D'Ercole et al., 2002; Garcia et al., 2014; Corvino et al., 2015; Wang et al., 2015). Collectively, these studies suggest that the function of Wnt-neuropeptide axis in synaptic assembly identified in *C. elegans* is most likely conserved in vertebrates.

An intrinsic role of gut in synaptic development

Using tissue-specific RNAi, tissue-specific rescue and transgenic GFP reporter experiments, we demonstrated that the Wnt-NLP-40 axis acts in the gut to regulate presynaptic assembly of nerve ring neurons. Further, we showed that the effect of the Wnt-NLP-40 axis on synaptic assembly at the newly hatched L1 stage, suggesting it acts during embryogenesis before feeding. We propose that the Wnt-NLP-40 axis acts through an intrinsic, stimulus-independent developmental program.

The gut-brain communication plays an important role in coping with unfavorite environmental conditions in *C. elegans*. For example, under stress conditions, intestinal SKN-1 regulates locomotion by modulating synaptic transmission at the neuromuscular junctions (D'Ercole et al., 2002; Staab et al., 2013). Insulin-like peptides INSs expressed in the intestine can regulate pathogen avoidance or feeding behavior through modulating the function of nervous system (Gruner et al., 2016; Lee and Mylonakis, 2017). Intestinal infections can affect the host's learning and behavior by neuroendocrine signaling pathways (Singh and Aballay, 2019). Intestinal immune responses can also protect neurons from degeneration (Chikka et al., 2016). However, the stimulus-independent role of gut-brain axis in the development is largely unexplored.

In vertebrates, the gut-brain-microbiota axis plays a vital role in mediating brain development and brain function, such as locomotion, exploratory and

risk-taking behaviors and spatial working and reference memory (Bercik et al., 2011; Diaz Heijtz et al., 2011; Gareau et al., 2011; Neufeld et al., 2011). Endocrine is a highly conserved signaling pathway mediated the gut-brain communication (Matafome et al., 2017; Farzi et al., 2018; Sun et al., 2018). Although it is unknown if gut-brain axis plays any intrinsic role in neural circuit formation in vertebrates, we posit that the signal pathway regulating synaptic formation is probably conserved given the conservation of gut-brain axis, Wnt signaling, neuroendocrine signaling.

Spontaneous neural activity regulates synaptic assembly

It is well known that neuroactivity regulates synaptic formation and plasticity (Hooks and Chen, 2020; Pan and Monje, 2020). Recently, we found that a pair of glutamatergic neurons regulates AIY synaptic subcellular specificity through inhibiting its activity during embryogenesis (Wang et al., 2021). The AIY presynaptic glutamate ASH neurons form synaptic connections at the AIY presynaptic posterior border. When the ASH neurons are overactivated, either by high temperature or overexpressing the vesicle glutamate transporter EAT-4, the AIY activity is suppressed through two glutamate gated choloride channels GLC-3 and GLC-4, which promotes ectopic synapse formation in the asynaptic region (Wang et al., 2021). Interestingly, here we found that Wnt-neuroendocrine signaling pathway is required for AIY spontaneously firing and presynaptic development, suggesting that this signaling pathway most likely regulates synaptic formation through activating the neurons.

Neuronal spontaneous activity is common during embryogenesis and plays critical roles in neuronal development including neurogenesis and circuit formation (Moody and Bosma, 2005; Blankenship and Feller, 2010). Based on our finding and studies from other groups, it is most likely that the role of neuronal spontaneous activity in synaptogenesis is conserved.

Collectively, our findings not only provide mechanistic insights into the synaptic assembly, but also uncovered a novel gut-brain interaction.

MATERIALS AND METHODS

Strains and maintenance

All *C. elegans* strains were grown with *E. coli* OP50 on standard NGM plates at 21°C. A detailed information of all the strains is listed in Supplementary Table S1. Animals were used in this study at adult day 1 stage unless specified The following strains were generated in our lab.

Plasmids and transformation

Constructs were made with either the pSM vector (derivation of pPD49.26) for transgene plasmid (Mello and Fire, 1995; Shen and Bargmann, 2003) or L4440 vector (derivation of pPD129.36) for RNAi (Kamath and Ahringer, 2003).

All endogenous and tissue specific *cfz-2, nlp-40* and *aex-2* rescue constructs were built with the pSM (Shen and Bargmann, 2003). Detailed information is described in Table S2.

To generate RNA interference (RNAi) constructs, cDNA was amplified and cloned into the double inverted T7 L4440 vector(Kamath and Ahringer, 2003). Detailed information is described in Table S2. Four NLP-40 mutant variants (M1 to M4, corresponding to the defective P1-P4 respectively) were constructed with three consecutive residues replaced with alanine in one of the predicted mature peptides. (M1 [(24' GLE) to AAA, we change the (70' ggtctcgag) to (gctgccgcg)]; M2 [(62' FVP) to AAA, (184' tttgttcca) to (gctgctgca)]; M3[(71' WQP) to AAA, (211' tggcagccg) to(gcggcggcg)]; M4[(109'PEE) to AAA, (325'ccggaggaa) to (gcggcggca)]) (Wang et al., 2013). Detailed information is described in Table S2. Transgenic strains were generated by microinjections as previously described (Mello and Fire, 1995).

We used P*hlh-17::mCherry*(20ng/μl), P*unc-122::gfp*(20ng/μl) or P*ttx-3::sl2::mCherry* (20ng/μl) as coinjection markers. Detailed information is described in Table S2.

RT and qRT-PCR

qRT-PCR was performed as the previous study (Shen et al., 2012). In brief, for mRNA, total RNA was prepared by traditional Trizol extraction methods from ~100 worms. cDNA was subsequently generated by GoScript™ Reverse Transcription system for RT-qPCR (Bio-Rad). qRT-PCR was performed with 2xNovoStart®SYBR qPCR SuperMix Plus (Novoprotein) on a CFX384 TouchTM Real-Time PCR Detection System (Bio-Rad). Three technical replicates were performed in each reaction. *nlp-40* was used as reference for mRNA quantification, the results were from at least three biological replicates. qRT-PCR primers for *nlp-40* was designed and was listed in Table S2.

RNA interference

RNAi constructs were transformed into HT115. RNAi feeding experiments were performed based on the previous study (Fraser et al., 2000). For tissue-specific RNAi experiment, we used the worm strain FDU2851(*sid-1(qt9); alxIs9[Pvha-6::sid-1::sl2::GFP]; olaIs12[Pttx-3::mCherry::rab-3; Phlh-17::GFP])* and FDU3111(*sid-1(pk3321); UIS69[Punc-119::sid-1; Pmyo-2::mCherry]; wyIs45[Pttx-3::GFP::rab-3; Punc-122::RFP])* for intestine and neuronal specific RNAi respectively. To screen the intestinal neuropeptide encoding genes through RNAi knockdown for the AIY presynaptic regulators, we transferred ten synchronized day 1 adults to the RNAi plates, allow them to lay eggs for two hours, then remove those adults. Then, we quantified the AIY synaptic fluorescent intensity at the adult day 1 stage.

In vivo calcium imaging

The animals FDU424(*olaIs17 [Pmod-1::GCaMP6; Pttx-3::mCherry; Punc-122::dsRed]*) and FDU3604 (*nlp-40(tm4085)*;*olaIs17 [Pmod-1::GCaMP6; Pttx-3::mCherry; Punc-122::dsRed]*) were used for calcium imaging in AIY interneurons. AIY^{ON} and AIY^{OFF} neurons were identified via expression of GCaMP6 driven under *mod-1* promoter. The P*ttx-3::mCherry* were selected for imaging to control for AIY expression. Calcium imaging of adult day 1 animals was performed on 10% agarose pads immobilized with 0.1 μm polystyrene beads and covered with glass coverslip.

Images were captured with Andor Dragonfly Spinning Disc Confocal Microscope with 60X objectives, 488 nm (for GFP) or 561 nm (for mCherry) laser. Individual animals were imaged for 60s at a rate of 2 Hz. Data were analyzed using custom written scripts in R Studio, and the images rotation and brightness/contrast were processed with Adobe photoshop CC. The 60s video was exported with Imaris 4.0.

Fluorescence microscope and confocal imaging

For microscopy experiments, worms were anesthetized on 3% agarose pads with 50 mM muscimol. Images were captured with Andor Dragonfly Spinning Disc Confocal Microscope with 10X or 40X objectives, 488 nm (for GFP) or 561 nm (for mCherry) laser. The fluorescence intensity was quantified with Imaris 4.0, and the images rotation and brightness/contrast were processed with Adobe photoshop CC.

Quantification and statistical analysis

We quantified the fluorescence intensity using Imaris. The density obtained by cropping the whole AIY interneuron zone (showed in Fig. 1A dashed box) and the whole intestinal zone and NR zone (showed in Fig. 7A dashed box) in

Imaris. To monitor the temporal role of indicated genes, we quantified the F1 animals' phenotype when F0 day1 animals' eggs laid and were synchronized as 12, 20, 30, 42, 66 hr later, respectively. All quantified data were collected from at least three biological replicates. For data with transgenic animals, at least two independent lines were used. The statistical P values were measured using GraphPad Prism 6.0 (GraphPad Software). Statistical analysis between two groups were based on Student's t-test (two-tailed), among more than two groups were based on one-way ANOVA followed by Dunnett's test, as indicated in the Fig. legends. All quantitative data were collected blindly.

ACKNOWLEDGMENTS

We thank ZF Altun and DH Hall from WormAtlas for help with schematic Fig.s. We thank Derek Sieburth (University of Southern California), Shiqing Cai, Yidong Shen (Chinese Academy of Sciences), Di Chen (Nanjing University), Huanhu Zhu (Shanghai tech), Zhao Qin (Tongji University) and Caenorhabditis Genetic Center funded by NIH (P40 OD010440) for providing strains or plasmids. We thank members in Shao laboratory for comments on the project. We thank Min Jang, Ying Shi, Mi Zhou from IOBS facility core at Fudan University for providing technical support on image acquisition. This study was supported by the National Natural Science Foundation of China (Grant No. 31471026), Shanghai Municipal Science and Technology Major Project (No. 2018SHZDZX01) and ZJLab. We thank Life Science Editors for editing assistance.

ABBREVIATIONS

GI, gastrointestinal; EECs, enteroendocrine cells; CCK, cholecystokinin; PYY, peptide tyrosine-tyrosine; GLP-1, glucagon-like peptide-1; RNAi, RNA interference; PC2, proprotein convertase; GPCR, G Protein-Coupled Receptor;

TCF, T-cell specific transcription factor; NLPs, neuropeptide-like proteins; ILPs, insulin-like peptides; FLPs, FMRFamide-related peptides.

COMPLIANCE WITH ETHICS GUIDELINES

The authors declare no competing interests. All institutional and national guidelines for the care and use of laboratory animals were followed.

AUTHOR CONTRIBUTIONS

YS and ZS conceived, designed the project. YS, LQ and ZS performed experiments and analyzed data, interpreted the results. YS and ZS wrote the manuscript.

REFERENCE

Bercik, P., Denou, E., Collins, J., Jackson, W., Lu, J., Jury, J., Deng, Y., Blennerhassett, P., Macri, J., McCoy, K.D.*, et al.* (2011). The intestinal microbiota affect central levels of brain-derived neurotropic factor and behavior in mice. Gastroenterology 141, 599-609, 609 e591-593.

Bernhard Kleine, and Rossmanith, W.G. Evolution of the Endocrine System. In Hormones and the Endocrine System (Cham, Springer), pp. 347-353.

Blankenship, A.G., and Feller, M.B. (2010). Mechanisms underlying spontaneous patterned activity in developing neural circuits. Nat Rev Neurosci 11, 18-29.

Budnik, V., and Salinas, P.C. (2011). Wnt signaling during synaptic development and plasticity. Curr Opin Neurobiol 21, 151-159.

Campbell, R.K., Satoh, N., and Degnan, B.M. (2004). Piecing together evolution of the vertebrate endocrine system. Trends Genet 20, 359-366.

Chew, Y.L., Grundy, L.J., Brown, A.E.X., Beets, I., and Schafer, W.R. (2018). Neuropeptides encoded by nlp-49 modulate locomotion, arousal and egg-laying behaviours in Caenorhabditis elegans via the receptor SEB-3. Philos Trans R Soc Lond B Biol Sci 373.

Chidambaram, S.B., Tuladhar, S., Bhat, A., Mahalakshmi, A.M., Ray, B., Essa, M.M., Bishir, M., Bolla, S.R., Nanjaiah, N.D., Guillemin, G.J.*, et al.* (2020). Autism and Gut-Brain Axis: Role of Probiotics. Adv Neurobiol 24, 587-600.

Chikka, M.R., Anbalagan, C., Dvorak, K., Dombeck, K., and Prahlad, V. (2016). The Mitochondria-Regulated Immune Pathway Activated in the C. elegans

Intestine Is Neuroprotective. Cell Rep 16, 2399-2414.
Colon-Ramos, D.A., Margeta, M.A., and Shen, K. (2007). Glia promote local synaptogenesis through UNC-6 (netrin) signaling in C-elegans. Science 318, 103-106.
Corvino, V., Di Maria, V., Marchese, E., Lattanzi, W., Biamonte, F., Michetti, F., and Geloso, M.C. (2015). Estrogen administration modulates hippocampal GABAergic subpopulations in the hippocampus of trimethyltin-treated rats. Front Cell Neurosci 9, 433.
Couillault, C., Pujol, N., Reboul, J., Sabatier, L., Guichou, J.F., Kohara, Y., and Ewbank, J.J. (2004). TLR-independent control of innate immunity in Caenorhabditis elegans by the TIR domain adaptor protein TIR-1, an ortholog of human SARM. Nature Immunology 5, 488-494.
Cryan, J.F., O'Riordan, K.J., Cowan, C.S.M., Sandhu, K.V., Bastiaanssen, T.F.S., Boehme, M., Codagnone, M.G., Cussotto, S., Fulling, C., Golubeva, A.V.*, et al.* (2019). The Microbiota-Gut-Brain Axis. Physiol Rev 99, 1877-2013.
D'Ercole, A.J., Ye, P., and O'Kusky, J.R. (2002). Mutant mouse models of insulin-like growth factor actions in the central nervous system. Neuropeptides 36, 209-220.
Davis, R.E., and Stretton, A.O.W. (2001). Structure-activity relationships of 18 endogenous neuropeptides on the motornervous system of the nematode Ascaris suum. Peptides 22, 7-23.
Diaz Heijtz, R., Wang, S., Anuar, F., Qian, Y., Bjorkholm, B., Samuelsson, A., Hibberd, M.L., Forssberg, H., and Pettersson, S. (2011). Normal gut microbiota modulates brain development and behavior. Proc Natl Acad Sci U S A 108, 3047-3052.
Dimaline, R., and Dockray, G.J. (1994). Evolution of the gastrointestinal endocrine system (with special reference to gastrin and CCK). Baillieres Clin Endocrinol Metab 8, 1-24.
Dockray, G.J. (2013). Enteroendocrine cell signalling via the vagus nerve. Curr Opin Pharmacol 13, 954-958.
Doshi, S., Price, E., Landis, J., Barot, U., Sabatella, M., Lans, H., and Kalb, R.G. (2019). Neuropeptide signaling regulates the susceptibility of developing C. elegans to anoxia. Free Radic Biol Med 131, 197-208.
Dreier, L., Burbea, M., and Kaplan, J.M. (2005). LIN-23-mediated degradation of beta-catenin regulates the abundance of GLR-1 glutamate receptors in the ventral nerve cord of C. elegans. Neuron 46, 51-64.
Farzi, A., Frohlich, E.E., and Holzer, P. (2018). Gut Microbiota and the

Neuroendocrine System. Neurotherapeutics 15, 5-22.
Fraser, A.G., Kamath, R.S., Zipperlen, P., Martinez-Campos, M., Sohrmann, M., and Ahringer, J. (2000). Functional genomic analysis of C. elegans chromosome I by systematic RNA interference. Nature 408, 325-330.
Garcia, I., Quast, K.B., Huang, L., Herman, A.M., Selever, J., Deussing, J.M., Justice, N.J., and Arenkiel, B.R. (2014). Local CRH signaling promotes synaptogenesis and circuit integration of adult-born neurons. Dev Cell 30, 645-659.
Garcia-Jimenez, C. (2010). Wnt and incretin connections. Vitam Horm 84, 355-387.
Garcia-Martinez, J.M., Chocarro-Calvo, A., Moya, C.M., and Garcia-Jimenez, C. (2009). WNT/beta-catenin increases the production of incretins by entero-endocrine cells. Diabetologia 52, 1913-1924.
Gareau, M.G., Wine, E., Rodrigues, D.M., Cho, J.H., Whary, M.T., Philpott, D.J., Macqueen, G., and Sherman, P.M. (2011). Bacterial infection causes stress-induced memory dysfunction in mice. Gut 60, 307-317.
Gruner, M., Grubbs, J., McDonagh, A., Valdes, D., Winbush, A., and van der Linden, A.M. (2016). Cell-Autonomous and Non-Cell-Autonomous Regulation of a Feeding State-Dependent Chemoreceptor Gene via MEF-2 and bHLH Transcription Factors. PLoS Genet 12, e1006237.
He, C.W., Liao, C.P., and Pan, C.L. (2018). Wnt signalling in the development of axon, dendrites and synapses. Open Biol 8.
Hooks, B.M., and Chen, C. (2020). Circuitry Underlying Experience-Dependent Plasticity in the Mouse Visual System. Neuron 106, 21-36.
Hu, Z., Pym, E.C., Babu, K., Vashlishan Murray, A.B., and Kaplan, J.M. (2011). A neuropeptide-mediated stretch response links muscle contraction to changes in neurotransmitter release. Neuron 71, 92-102.
Hu, Z., Vashlishan-Murray, A.B., and Kaplan, J.M. (2015). NLP-12 engages different UNC-13 proteins to potentiate tonic and evoked release. J Neurosci 35, 1038-1042.
Husson, S.J., Clynen, E., Baggerman, G., De Loof, A., and Schoofs, L. (2005). Discovering neuropeptides in Caenorhabditis elegans by two dimensional liquid chromatography and mass spectrometry. Biochem Biophys Res Commun 335, 76-86.
Jensen, M., Hoerndli, F.J., Brockie, P.J., Wang, R., Johnson, E., Maxfield, D., Francis, M.M., Madsen, D.M., and Maricq, A.V. (2012). Wnt signaling regulates

acetylcholine receptor translocation and synaptic plasticity in the adult nervous system. Cell 149, 173-187.
Kamath, R.S., and Ahringer, J. (2003). Genome-wide RNAi screening in Caenorhabditis elegans. Methods 30, 313-321.
Kim, J.T., Liu, C., Zaytseva, Y.Y., Weiss, H.L., Townsend, C.M., Jr., and Evers, B.M. (2015). Neurotensin, a novel target of Wnt/beta-catenin pathway, promotes growth of neuroendocrine tumor cells. Int J Cancer 136, 1475-1481.
Klassen, M.P., and Shen, K. (2007). Wnt signaling positions neuromuscular connectivity by inhibiting synapse formation in C-elegans. Cell 130, 704-716.
Kowalski, K., and Mulak, A. (2019). Brain-Gut-Microbiota Axis in Alzheimer's Disease. J Neurogastroenterol Motil 25, 48-60.
Lee, K., and Mylonakis, E. (2017). An Intestine-Derived Neuropeptide Controls Avoidance Behavior in Caenorhabditis elegans. Cell Rep 20, 2501-2512.
Li, C. (2005). The ever-expanding neuropeptide gene families in the nematode Caenorhabditis elegans. Parasitology 131 Suppl, S109-127.
Li, C., and Kim, K. (2008). Neuropeptides. WormBook, 1-36.
Li, Q., and Zhou, J.M. (2016). The microbiota-gut-brain axis and its potential therapeutic role in autism spectrum disorder. Neuroscience 324, 131-139.
Luo, L., Cook, N., Venkatachalam, V., Martinez-Velazquez, L.A., Zhang, X., Calvo, A.C., Hawk, J., MacInnis, B.L., Frank, M., Ng, J.H.*, et al.* (2014). Bidirectional thermotaxis in Caenorhabditis elegans is mediated by distinct sensorimotor strategies driven by the AFD thermosensory neurons. Proc Natl Acad Sci U S A 111, 2776-2781.
Matafome, P., Eickhoff, H., Letra, L., and Seica, R. (2017). Neuroendocrinology of Adipose Tissue and Gut-Brain Axis. Adv Neurobiol 19, 49-70.
Mello, C., and Fire, A. (1995). DNA transformation. Methods Cell Biol 48, 451-482.
Mizumoto, K., and Shen, K. (2013). Two Wnts instruct topographic synaptic innervation in C. elegans. Cell Rep 5, 389-396.
Moody, W.J., and Bosma, M.M. (2005). Ion channel development, spontaneous activity, and activity-dependent development in nerve and muscle cells. Physiol Rev 85, 883-941.
Mulak, A., and Bonaz, B. (2015). Brain-gut-microbiota axis in Parkinson's disease. World J Gastroenterol 21, 10609-10620.
Nassel, D.R., Zandawala, M., Kawada, T., and Satake, H. (2019). Tachykinins: Neuropeptides That Are Ancient, Diverse, Widespread and Functionally

Pleiotropic. Front Neurosci 13, 1262.
Nathoo, A.N., Moeller, R.A., Westlund, B.A., and Hart, A.C. (2001). Identification of neuropeptide-like protein gene families in Caenorhabditiselegans and other species. Proc Natl Acad Sci U S A 98, 14000-14005.
Neufeld, K.M., Kang, N., Bienenstock, J., and Foster, J.A. (2011). Reduced anxiety-like behavior and central neurochemical change in germ-free mice. Neurogastroenterol Motil 23, 255-264, e119.
Oliva, C.A., and Inestrosa, N.C. (2015). A novel function for Wnt signaling modulating neuronal firing activity and the temporal structure of spontaneous oscillation in the entorhinal-hippocampal circuit. Exp Neurol 269, 43-55.
Pan, Y., and Monje, M. (2020). Activity Shapes Neural Circuit Form and Function: A Historical Perspective. J Neurosci 40, 944-954.
Pandey, P., Bhardwaj, A., and Babu, K. (2017). Regulation of WNT Signaling at the Neuromuscular Junction by the Immunoglobulin Superfamily Protein RIG-3 in Caenorhabditis elegans. Genetics 206, 1521-1534.
Park, M., and Shen, K. (2012). WNTs in synapse formation and neuronal circuitry. EMBO J 31, 2697-2704.
Pauli, F., Liu, Y., Kim, Y.A., Chen, P.J., and Kim, S.K. (2006). Chromosomal clustering and GATA transcriptional regulation of intestine-expressed genes in C. elegans. Development 133, 287-295.
Quigley, E.M.M. (2017). Microbiota-Brain-Gut Axis and Neurodegenerative Diseases. Curr Neurol Neurosci Rep 17, 94.
Reinitz, C.A., Herfel, H.G., Messinger, L.A., and Stretton, A.O.W. (2000). Changes in locomotory behavior and cAMP produced in Ascaris suum by neuropeptides from Ascaris suum or Caenorhabditis elegans. Molecular and Biochemical Parasitology 111, 185-197.
Shao, Z., Watanabe, S., Christensen, R., Jorgensen, E.M., and Colon-Ramos, D.A. (2013). Synapse Location during Growth Depends on Glia Location. Molecular Biology of the Cell 24.
Shen, K., and Bargmann, C.I. (2003). The immunoglobulin superfamily protein SYG-1 determines the location of specific synapses in C. elegans. Cell 112, 619-630.
Shen, Y., Wollam, J., Magner, D., Karalay, O., and Antebi, A. (2012). A steroid receptor-microRNA switch regulates life span in response to signals from the gonad. Science 338, 1472-1476.
Shi, Y., Li, Q., and Shao, Z. (2018). Wnts Promote Synaptic Assembly Through

T-Cell Specific Transcription Factors in Caenorhabditis elegans. Front Mol Neurosci 11, 194.
Singh, J., and Aballay, A. (2019). Intestinal infection regulates behavior and learning via neuroendocrine signaling. Elife 8.
Spencer, W.C., Zeller, G., Watson, J.D., Henz, S.R., Watkins, K.L., McWhirter, R.D., Petersen, S., Sreedharan, V.T., Widmer, C., Jo, J.*, et al.* (2011). A spatial and temporal map of C. elegans gene expression. Genome Res 21, 325-341.
Staab, T.A., Griffen, T.C., Corcoran, C., Evgrafov, O., Knowles, J.A., and Sieburth, D. (2013). The conserved SKN-1/Nrf2 stress response pathway regulates synaptic function in Caenorhabditis elegans. PLoS Genet 9, e1003354.
Sun, E.W.L., Martin, A.M., Young, R.L., and Keating, D.J. (2018). The Regulation of Peripheral Metabolism by Gut-Derived Hormones. Front Endocrinol (Lausanne) 9, 754.
Wang, H., Girskis, K., Janssen, T., Chan, J.P., Dasgupta, K., Knowles, J.A., Schoofs, L., and Sieburth, D. (2013). Neuropeptide secreted from a pacemaker activates neurons to control a rhythmic behavior. Curr Biol 23, 746-754.
Wang, H.X., and Wang, Y.P. (2016). Gut Microbiota-brain Axis. Chin Med J (Engl) 129, 2373-2380.
Wang, L., Chang, X., She, L., Xu, D., Huang, W., and Poo, M.M. (2015). Autocrine action of BDNF on dendrite development of adult-born hippocampal neurons. J Neurosci 35, 8384-8393.
Wang, M., Witvliet, D., Wu, M., Kang, L., and Shao, Z. (2021). Temperature regulates synaptic subcellular specificity mediated by inhibitory glutamate signaling. PLoS Genet 17, e1009295.
White, J.G., Southgate, E., Thomson, J.N., and Brenner, S. (1986). The Structure of the Nervous-System of the Nematode Caenorhabditis-Elegans. Philosophical Transactions of the Royal Society B-Biological Sciences 314, 1-340.

Figures and Figure legends:

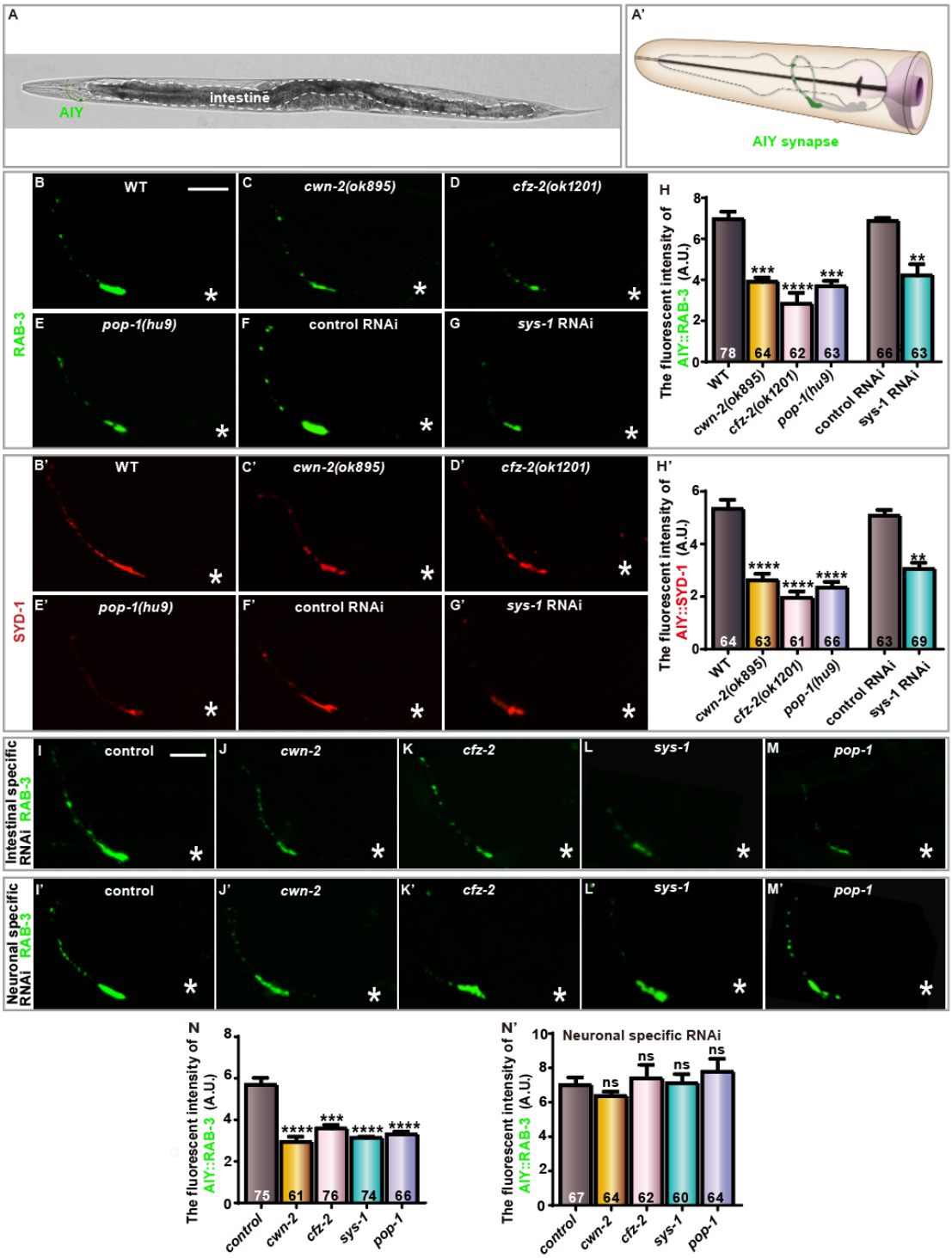

Fig. 1 AIY presynaptic assembly requires Intestinal Wnt signaling. (A) A bright field image of a wild-type adult *C. elegans*; the position of the AIY interneurons in the head are indicated with green color, and the intestine is outlined with dashed lines. (A') A cartoon diagram of the *C. elegans* head modified from wormatlas with permission. The AIY processes and soma are indicated in grey, and the AIY presynaptic sites are marked with green spots

(Altun et al., 2002–2019). (B-G') Confocal images of the AIY presynaptic structure labeled with the synaptic vesicle maker GFP::RAB-3(B-G, green) and synaptic active zone maker GFP::SYD-1(B'-G', pseudo-red) in wild-type (B, B'), *cwn-2(ok895)* (C, C'), *cfz-2(ok1201)* (D, D'), *pop-1(hu9)* (E, E'), and *sys-1* RNAi (G, G') animals. The scale bar in (B) is 10 μm and applied to (C-G'). (H-H') Quantification of fluorescent intensity of RAB-3 (H) and SYD-1 (H') for the indicated genotypes. Data are averaged from at least three biological replicates. The total number (N) of independent animals assayed is indicated in the bars. Statistical analyses are based on one-way ANOVA followed by Dunnett's test (for mutants) and two-tailed Student's t-test (for RNAi). **$p<0.01$, ***$p<0.001$, ****$p<0.0001$ as compared to WT or control RNAi. Error bars represent 95% confidence interval and SEM respectively. (I-M') Confocal images of AIY synaptic marker mCherry::RAB-3 (pseudo-GFP) of intestinal-specific RNAi (I-M) or GFP::RAB-3 of neuronal-specific RNAi (I'-M') treatment for control (I-I'), *cwn-2*(J-J'), *cfz-2*(K-K'), *sys-1*(L-L') and *pop-1*(M-M'). The scale bar in (I) is 10 μm and applied to (J-M'). (N-N') Quantification of GFP::RAB-3 fluorescent intensity for the indicated RNAi treatment. Data are averaged from at least three biological replicates. The total number (N) of independent animals assayed is indicated in the bars. Statistical analyses are based on one-way ANOVA followed by Dunnett's test. ns: not significance ($p>0.05$), ***$p<0.001$, ****$p<0.0001$ as compared to the control RNAi. Error bars represent 95% confidence interval.

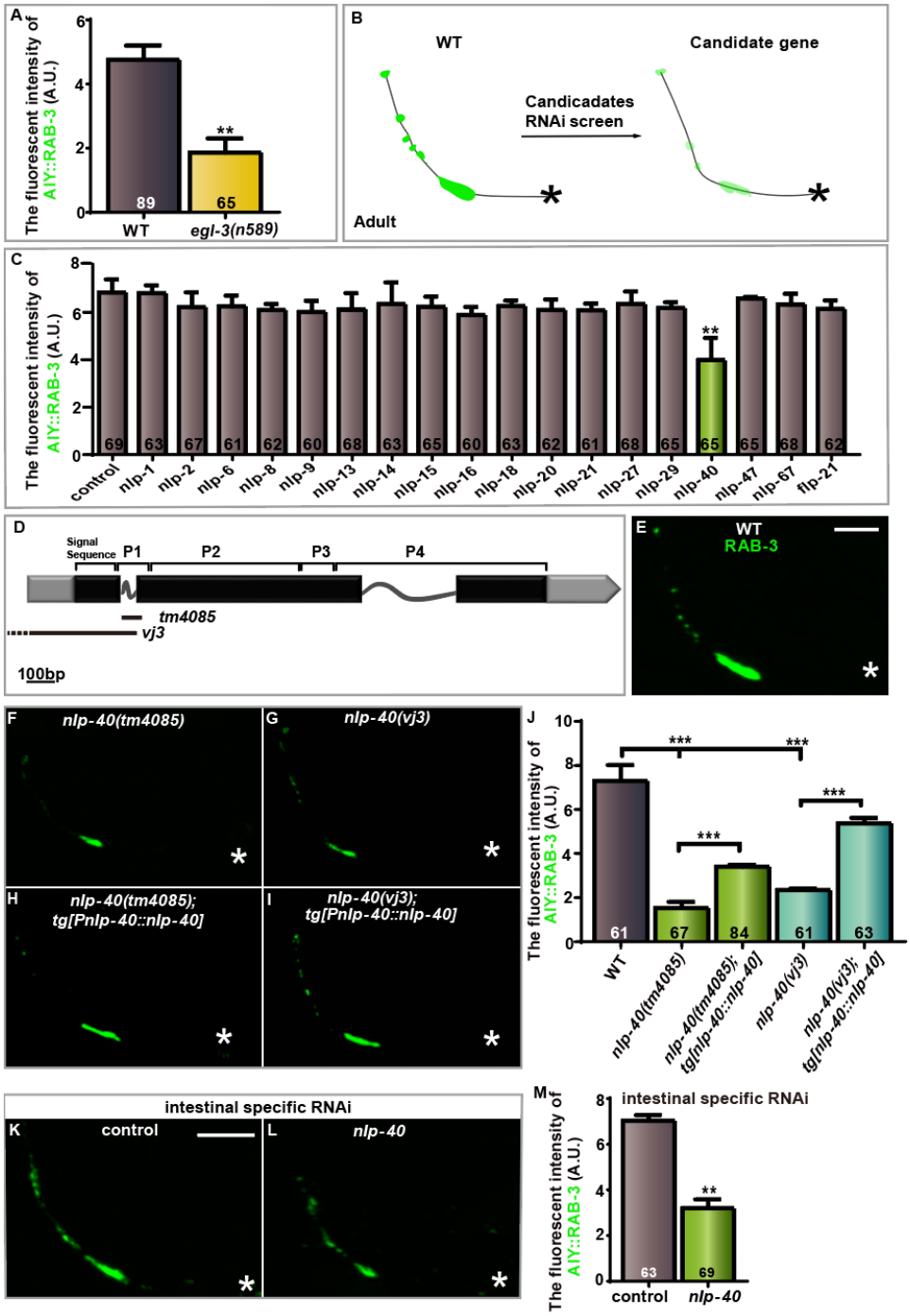

Fig. 2 AIY presynaptic assembly requires intestinal expressed *nlp-40*.

(A) Quantification of GFP::RAB-3 fluorescent intensity in wild-type and *egl-3(n589)* mutants. Data are averaged from at least three biological replicates. The total number (N) of independent animals assayed is indicated in the bars. Statistical analyses are based on two-tailed Student's t-test. **p<0.01. Error bars represent SEM. (B) A Schematic diagram describes the RNAi screen strategy to identify intestinal neuropeptides required for AIY synaptogenesis.

(C) Quantification of GFP::RAB-3 fluorescent intensity for the indicated RNAi treatment. Candidate genes are intestinal expressed *nlp* or *flp*. Data are averaged from at least three biological replicates. The total number (N) of independent animals assayed is indicated in the bars. Statistical analyses are based on one-way ANOVA followed by Dunnett's test. **$p<0.01$ as compared to the control RNAi. Error bars represent 95% confidence interval. (D) Diagram of *nlp-40* genomic structure. P1 to P4 indicates the predicted mature products of NLP-40. The boxes and lines represent exons and introns. Black and gray indicate coding sequence and UTRs. The lines beneath indicate the deletion region. (E-I) Confocal images of AIY synaptic marker GFP::RAB-3 in wild-type (E), *nlp-40(tm4085)* (F), *nlp-40(vj3)* (G), *nlp-40(tm4085)* (H) or *nlp-40(vj3)* (I) with wild type copy of *nlp-40*. Scale bars: 10 μm for all panels. (J) Quantification of GFP::RAB-3 fluorescent intensity for the indicated genotypes. Data are averaged from at least three biological replicates. Transgenic data are averaged from at least two independent lines. The total number (N) of independent animals assayed is indicated in the bars. Statistical analyses are based on one-way ANOVA followed by Dunnett's test. ***$p<0.001$. Error bars represent 95% confidence interval. (K-L) Confocal images of AIY synaptic marker GFP::RAB-3 for the indicated intestinal-specific RNAi treatment. The scale bar in (K) is 10μm and applies to (L). (M) Quantification of AIY GFP::RAB-3 fluorescent intensity for (K) and (L). Data for each genotype are averaged from at least three biological replicates. The total number (N) of independent animals assayed is indicated in the bars. Statistical analyses are based on two-tailed Student's t-test. **$p<0.01$. Error bars represent SEM.

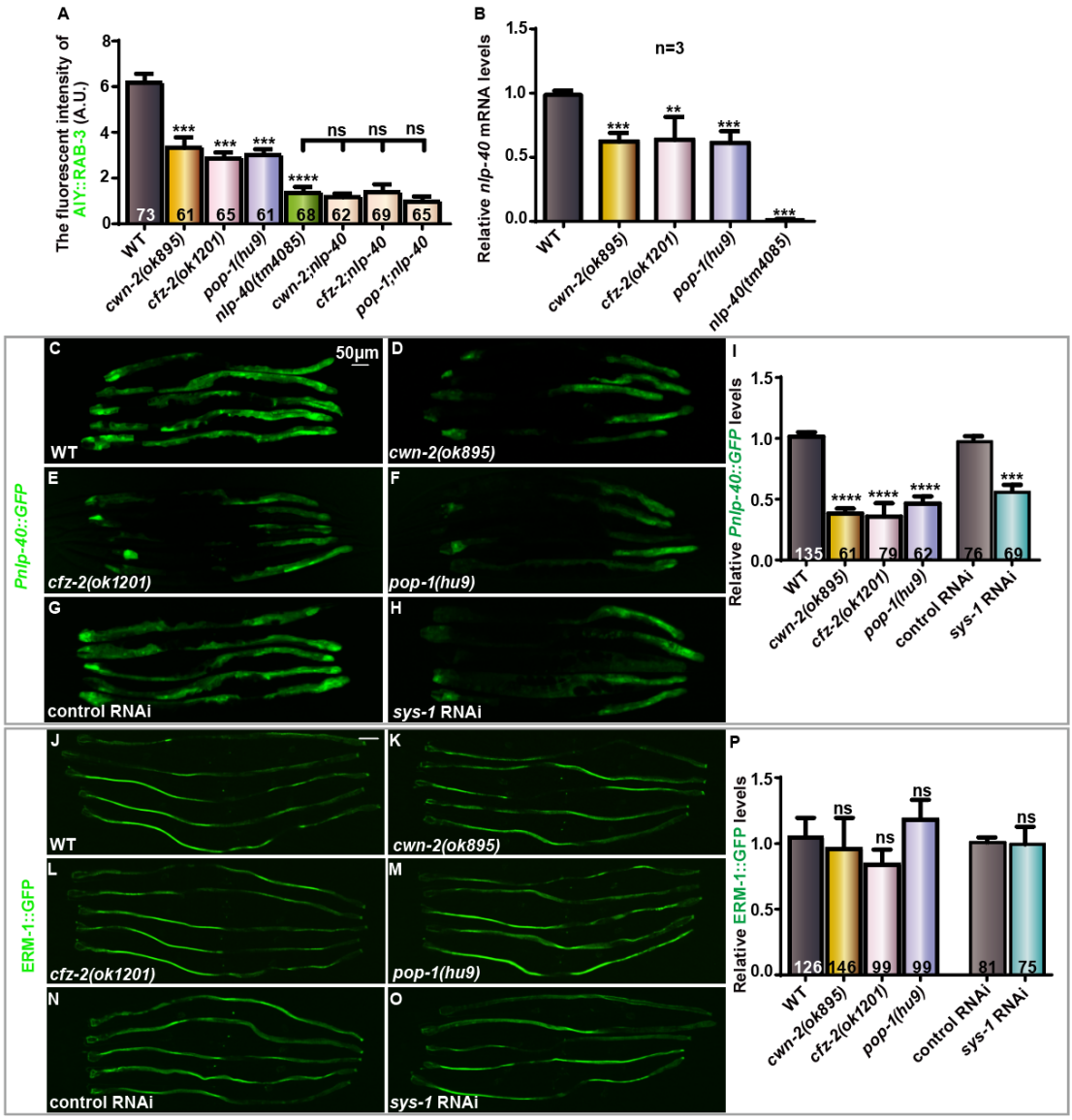

Fig. 3 Wnt signaling regulates AIY presynaptic assembly by promoting *nlp-40* expression. (A) Quantification of the fluorescent intensity of AIY presynaptic marker GFP::RAB-3 for the indicated genotypes. The double mutant data shows that *nlp-40(tm4085)* is epistatic to all Wnt mutants, indicating that *nlp-40* acts downstream of Wnt signaling. Data are averaged from at least three biological replicates. The total number (N) of independent animals assayed is indicated in the bars. Statistical analyses are based on one-way ANOVA followed by Dunnett's test. ns: not significance (p>0.05); ***p<0.001; ****p<0.0001. Error bars represent 95% confidence interval. (B) Quantification of *nlp-40* mRNA level for the indicated genotypes. The *nlp-40* mRNA is robustly reduced in *cwn-2(ok895)*, *cfz-2(ok1201)*, or *pop-1(hu9)* mutants. Data are averaged from three biological replicates. The total number (N) of independent animals assayed is indicated in the bars. Statistical

analyses are based on one-way ANOVA followed by Dunnett's test. **p<0.01; ***p<0.001 as compared with wild-type. Error bars represent 95% confidence interval. (C-H) Confocal images of the transcriptional *nlp-40* reporter (*Pnlp-40::GFP*) in wild-type (C), *cwn-2(ok895)* (D), *cfz-2(ok1201)* (E), *pop-1(hu9)* (F), and control or *sys-1* RNAi (G and H) animals at adult Day 1 stage. Scale bars: 50 μm. (I) Quantification of P*nlp-40::GFP* fluorescent intensity for the indicated genotypes. Data are averaged from at least three biological replicates. The total number (N) of independent animals assayed is indicated in the bars. Statistical analyses are based on one-way ANOVA followed by Dunnett's test (for mutants) and two-tailed Student's t-test (for RNAi). ***p<0.001, ****p<0.0001 as compared to WT or control RNAi. Error bars represent 95% confidence interval and SEM respectively. (J-O) Confocal images of an intestinal-specific reporter ERM-1::GFP in wild-type (J), *cwn-2(ok895)* (K), *cfz-2(ok1201)* (L), *pop-1(hu9)* (M), and control or *sys-1* RNAi (N and O) animals at adult Day1 stage. Scale bars: 50μm. (P) Quantification of ERM-1::GFP fluorescent intensity for the indicated genotype. Data are averaged from at least three biological replicates. The total number (N) of independent animals assayed is indicated in the bars. Statistical analyses are based on one-way ANOVA followed by Dunnett's test (for mutants) and two-tailed Student's t-test (for RNAi). ns: not significant as compared to WT or control RNAi (p>0.05). Error bars represent 95% confidence interval and SEM respectively.

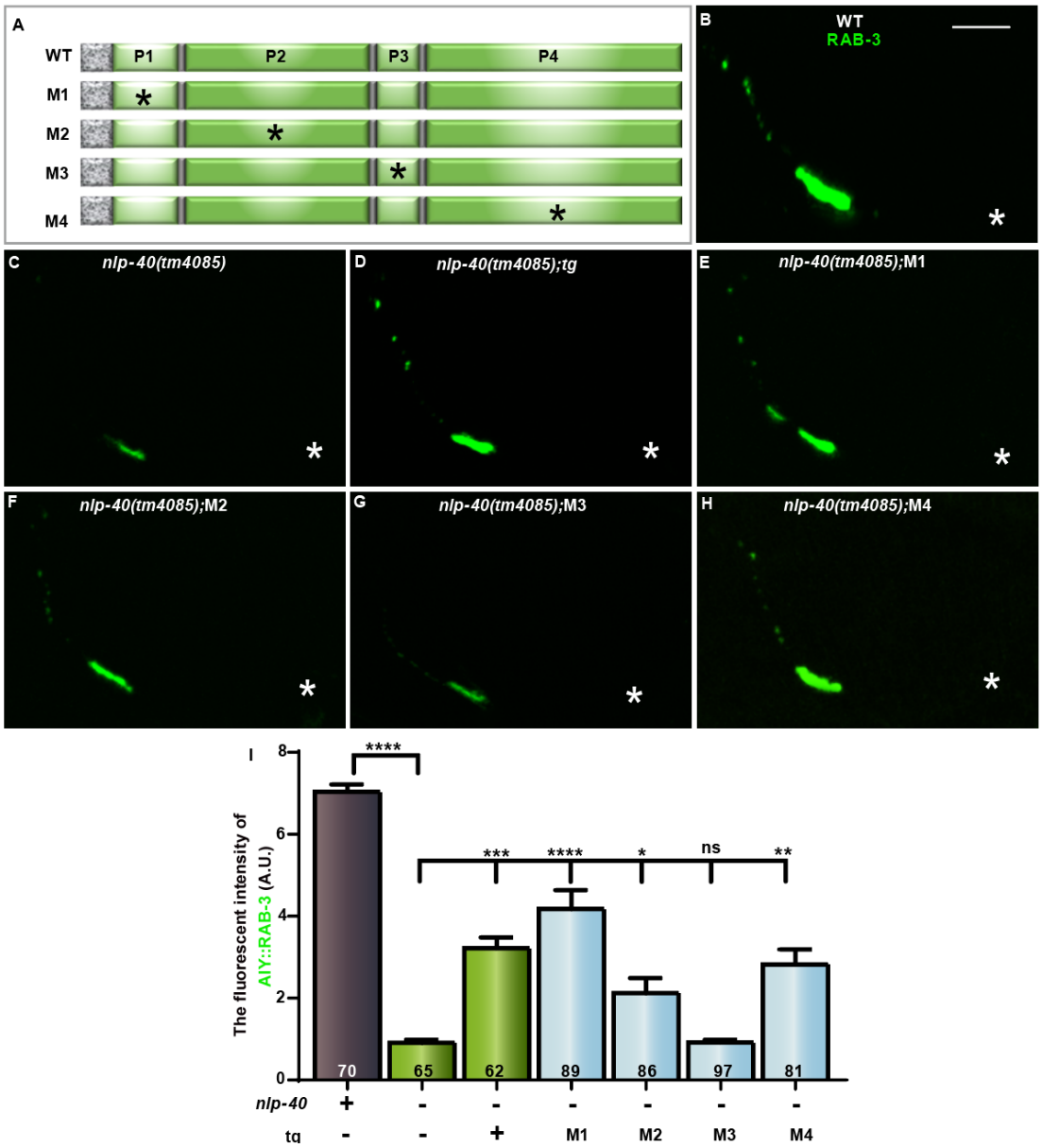

Fig. 4 AIY presynaptic assembly requires peptide P3 derived from NLP-40. (A) Schematic of the neuropeptide precursor protein NLP-40. P1-P4 are predicted mature peptides derived from NLP-40 (Wang et al 2013), WT: *Pnlp-40::nlp-40*. Marble regions represent signal sequences, M1-M4 are missense mutations inactivating P1-P4 respectively. (M1 [(24' GLE) to AAA]; M2 [(62' FVP) to AAA]; M3[(71' WQP) to AAA]; M4[(109'PEE) to AAA]). (B-H) Confocal images of AIY GFP::RAB-3 in wild-type (B), *nlp-40 (tm4085)* (C), and the *nlp-40(tm4085)* with *Pnlp-40::nlp-40* (WT) (D), with *Pnlp-40::nlp-40* (M1) (E), with *Pnlp-40::nlp-40* (M2) (F), with *Pnlp-40::nlp-40* (M3) (G), with *Pnlp-40::nlp-40* (M4) (H). (I) Quantification of AIY GFP::RAB-3 fluorescent intensity for the indicated genotypes. tg: P*nlp-40::nlp-40* cDNA transgene, +: wild type, -: mutant or without tg. Data are averaged from at least three biological replicates. M1-M4 indicate the mutant forms of NLP-40 as indicated

in (A). Transgenic data are averaged from at least two independent lines. The total number (N) of independent animals assayed is indicated in the bars. Statistical analyses are based on one-way ANOVA followed by Dunnett's test. ns: not significance ($p>0.05$), *$p<0.05$, **$p<0.01$, ***$p<0.001$, ****$p<0.0001$. Error bars represent 95% confidence interval.

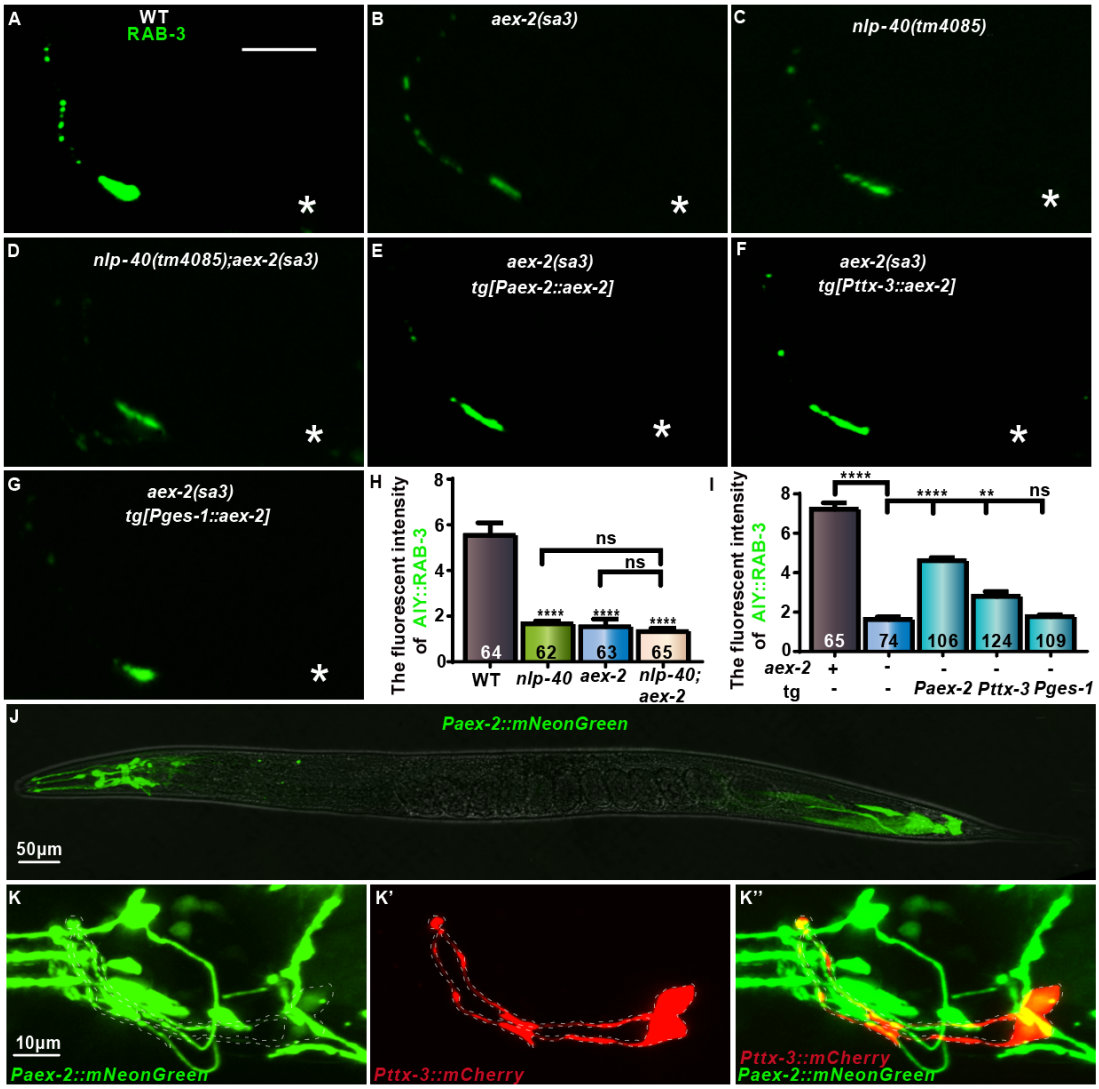

Fig. 5 NLP-40 receptor AEX-2 is required for AIY presynaptic assembly. (A-G) Confocal images of AIY GFP::RAB-3 in wild type (A), *aex-2(sa3)* (B), *nlp-40(tm4085)* (C) and *nlp-40(tm4085);aex-2(sa3)*(D) mutants and *aex-2(sa3)* with an *aex-2* transgene driven by the endogenous promoter(*Paex-2*) (E), AIY-specific promoter (*Pttx-3*) (F) transgene or intestinal-specific promoter (*Pges-1*) (G). The scale bar in (A) is 10μm and applies to (B-G). (H-I) Quantification of AIY GFP::RAB-3 fluorescent intensity for the indicated genotypes. Data are averaged from at least three biological replicates. Transgenic data are averaged from at least two independent lines. The total number (N) of independent animals assayed is indicated in the bars. Statistical analyses are based on one-way ANOVA followed by Dunnett's test and two-tailed Student's t-test. tg: *Paex-2::aex-2, Pttx-3::aex-2 or Pges-1::aex-2* transgene, +: wild type ; -: mutant or without tg, ns: not significance (p>0.05), **p<0.01, ****p<0.0001. Error bars represent 95% confidence interval or SEM

respectivelly. (J-K'') Confocal images of *Paex-2*::mNeonGreen of whole animal with bright field (J), the head with *Paex-2*::mNeonGreen and *Pttx-3*::mCherry with green channel (K), red channel (K') and the merged channels (K''). The scale bar in (J) is 50μm; The scale bar in (K) is 10μm and applies to (K' and K'').

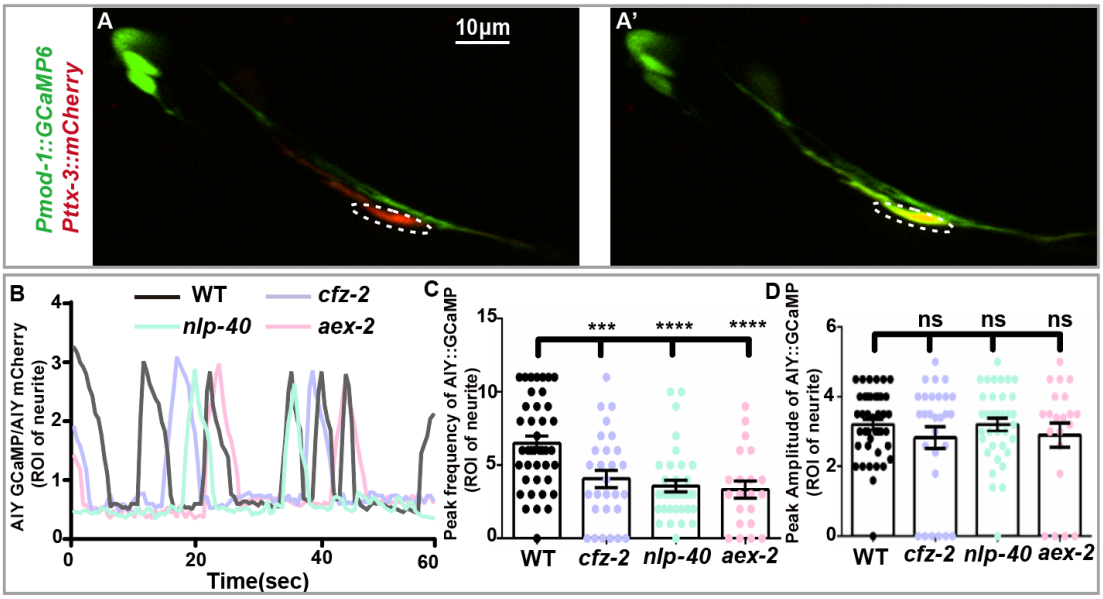

Fig. 6 NLP-40 is required for the excitation of AIY interneurons. (A-A') Representative confocal images showing GCaMP6 (with *mod-1* promoter) OFF(A) and ON(A') of AIY interneuron colabeled with mCherry (with *ttx-3* promoter) (red). Dashed ovals mark the AIY presynaptic enriched region where GCaMP was quantified. The scale bar in (A-A') is 10μm. (B) Representative AIY calcium activity over 60 seconds for WT, *cfz-2(ok1201)*, *nlp-40(tm4085)* and *aex-2(sa3)* mutant animals. (C-D) Quantification of the peak frequency and amplitude of AIY::GCaMP6 in WT, *cfz-2(ok1201)*, *nlp-40(tm4085)* and *aex-2(sa3)* mutants. Each spot represents the data from one animal. Data are averaged from at least three biological replicates. Statistical analyses are based on one-way ANOVA followed by Dunnett's test. ns: not significance ($p>0.05$); ***$p<0.001$, ****$p<0.0001$. Error bars represent 95% confidence interval.

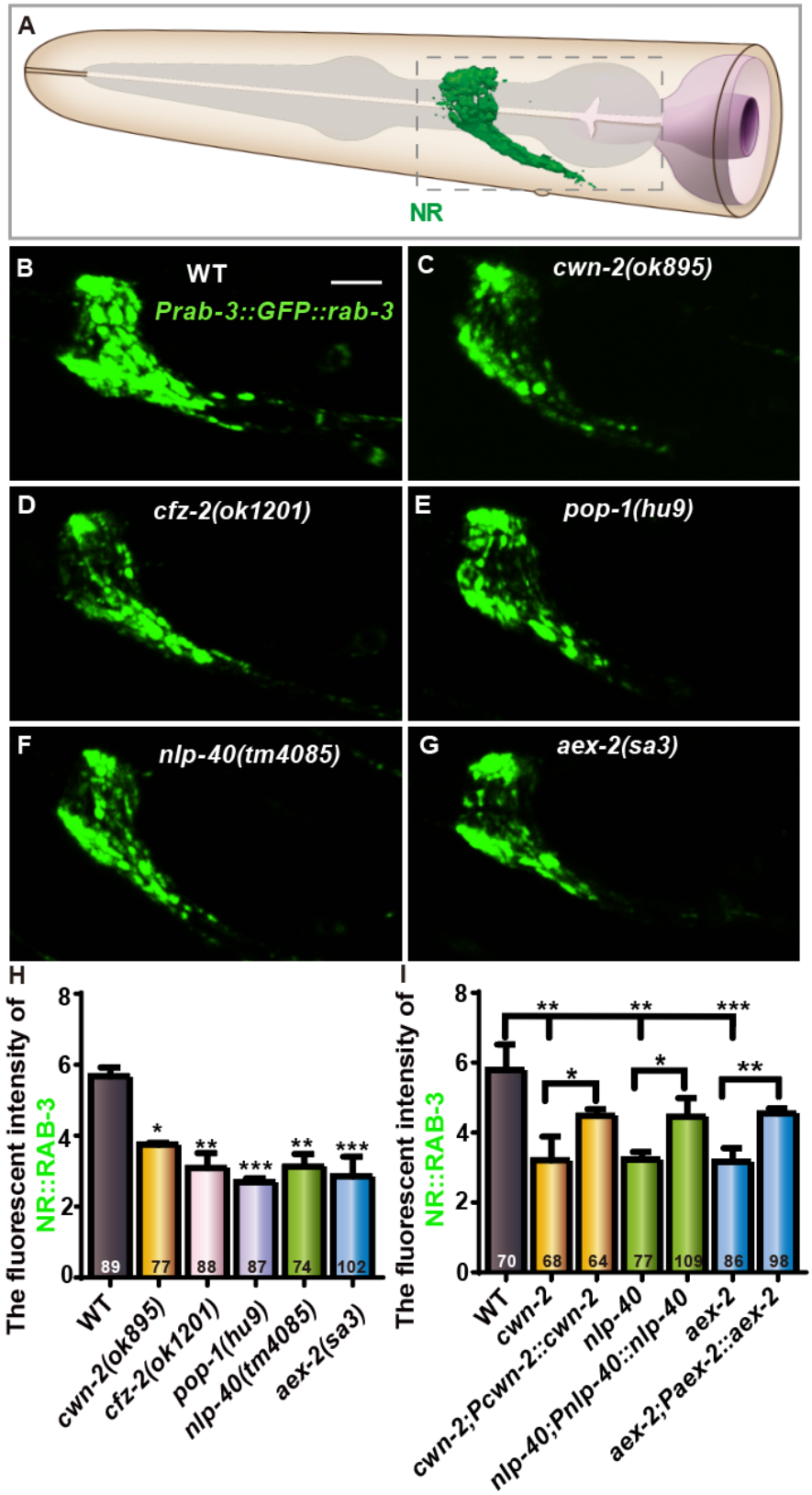

Fig. 7 Synaptic assembly in the nerve ring requires both Wnts and NLP-40 neuropeptide signaling. (A) A cartoon diagram of the *C. elegans* head. Green marks the presynaptic region in the nerve ring. (B-G) Confocal images of *Prab-3::GFP::rab-3* in the nerve region (corresponding the dashed

box in (A) of wild type (B), *cwn-2(ok895)*(C)*, cfz-2(ok1201)*(D), *pop-1(hu9)*(E), *nlp-40(tm4085)*(F) and *aex-2(sa3)*(G) mutants. The scale bar in (B) is 10μm, applies to (C-G). (H-I) Quantification of the GFP intensity in the nerve ring for the indicated genotypes. Data for each genotype are averaged from at least three biological replicates. Transgenic data are averaged from at least two independent lines. The total number (N) of independent animals assayed is indicated in the bars. Statistical analyses are based on one-way ANOVA followed by Dunnett's test and two-tailed Student's t-test. *$p<0.05$, **$p<0.01$, ***$p<0.001$. Error bars represent 95% confidence interval and SEM respectively.

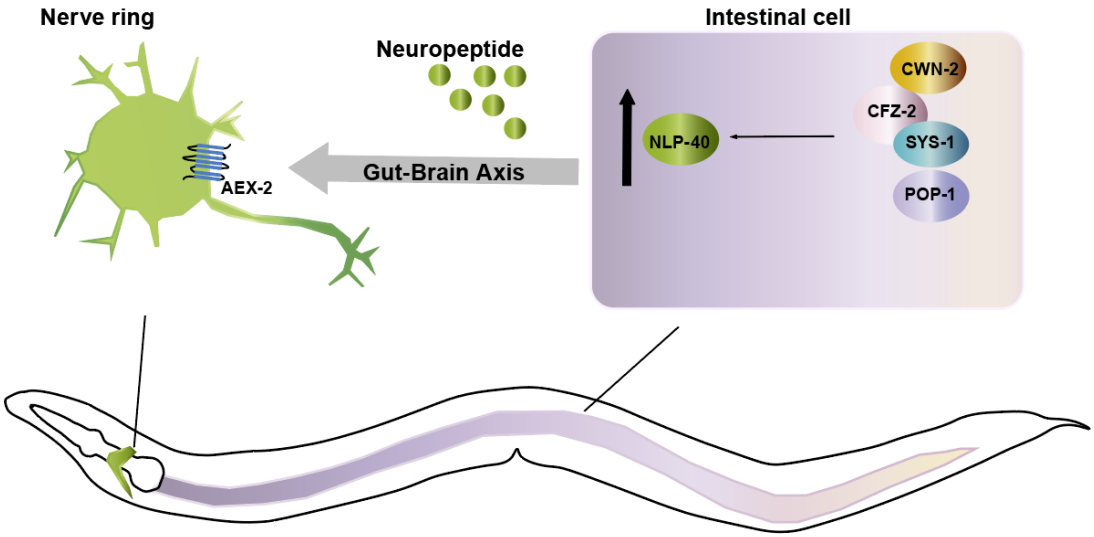

Fig. 8 A model describing synaptic assembly mediated by Intrinsic Wnt-neuropeptide signaling from gut. A canonical Wnt signaling pathway including Wnt/CWN-2, Frizzled/CFZ-2, β-catenin/SYS-1 and TCF/POP-1 acts in the intestine to promote the synaptic assembly in the *C. elegans* nerve ring, a structure analogous to the mammalian brain. Wnt signaling upregulates the expression of *nlp-40*, which encodes a conserved neuropeptide. NLP-40 is secreted outside the intestine and triggers the synaptic assemble through the neuronal expressed receptor GPCR/AEX-2.

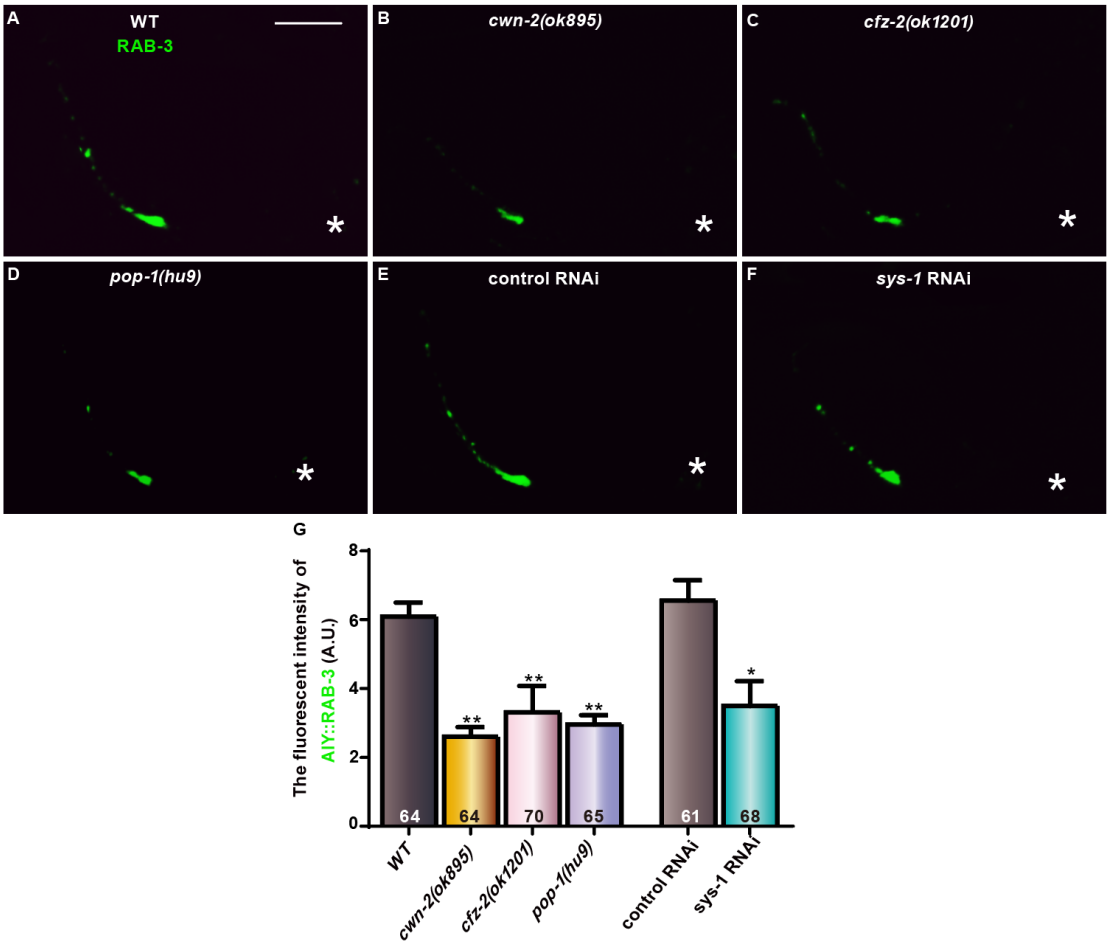

Supplementary Fig. 1 AIY presynaptic assembly requires canonical Wnt signaling components. (A-F) Confocal images of AIY synaptic marker mCherry::RAB-3 (pseudogreen) in wild type(A), *cwn-2(ok895)*(B), *cfz-2(ok1201)*(C), *pop-1(hu9)*(D) mutants, empty vector control (E) and *sys-1* RNAi (F) animals. The fluorescent intensity is significantly reduced in *cwn-2(ok895)*, *cfz-2(ok1201)*, *pop-1(hu9)*, or *sys-1* RNAi animals. Asterisks indicate AIY soma. The scale bar in (A) is 10μm, applying for all image panels. (G) Quantification of the fluorescent intensity of AIY RAB-3 for the indicated genotypes. Data are averaged from at least three biological replicates. The total number (N) of independent animals assayed is indicated in the bars. Statistical analyses are based on one-way ANOVA followed by Dunnett's test (for mutants) or two-tailed Student's t-test (for RNAi). *p<0.05, **p<0.01 as compared to WT or control RNAi. Error bars represent 95% confidence interval or SEM respectivelly.

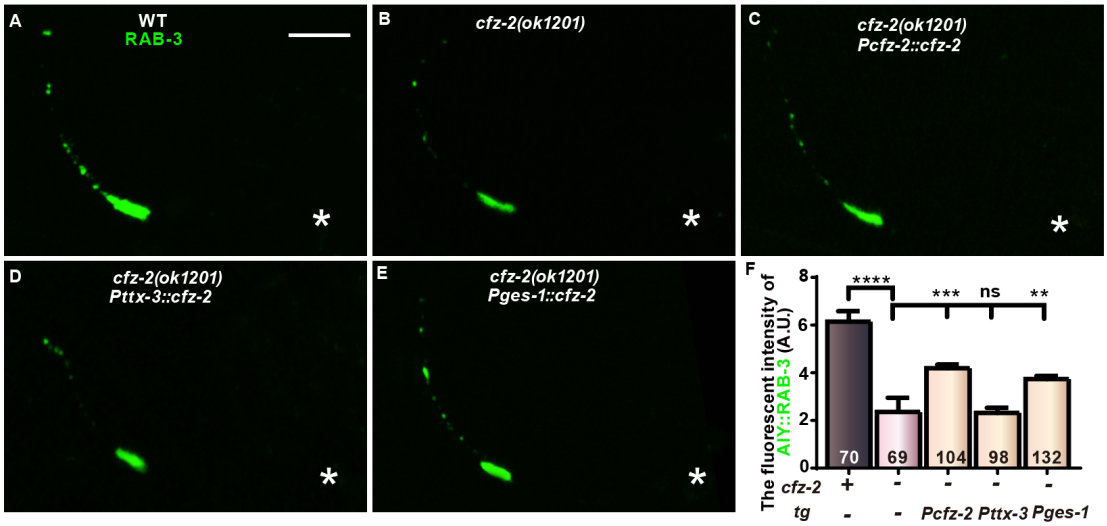

Supplementary Fig. 2 AIY presynaptic assembly requires intestinal *cfz-2*. (A-E) Confocal images of AIY GFP::RAB-3 in wild type (A), *cfz-2(ok1201)* (B), *cfz-2(ok1201)* with an *cfz-2* transgene expressed with endogenous promoter(*Pcfz-2*) (C), AIY-specific promoter (*Pttx-3*) (D) or intestine-specific promoter (*Pges-1*) (E) transgene. The scale bar in (A) is 10μm and applies to (B-E). (F) Quantification of AIY GFP::RAB-3 fluorescent intensity for the indicated genotypes. Data are averaged from at least three biological replicates. Transgenic data are averaged from at least two independent lines. The total number (N) of independent animals assayed is indicated in the bars. Statistical analyses are based on one-way ANOVA followed by Dunnett's test. ns: not significant ($p>0.05$), **$p<0.01$, ***$p<0.001$, ****$p<0.0001$. Error bars represent 95% confidence interval.

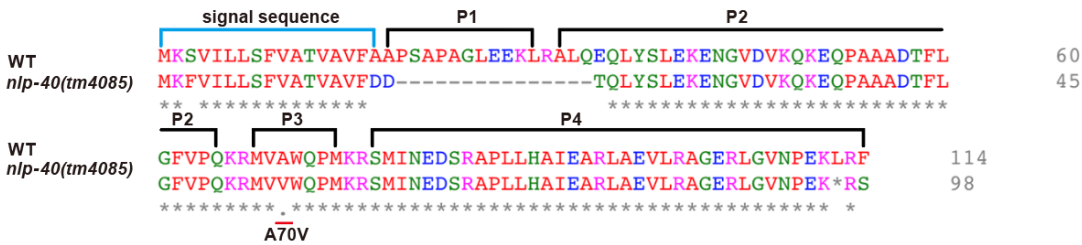

Supplementary Fig. 3 Protein alignment of NLP-40 and loss of function mutants *nlp-40(tm4085)*. The image represents the protein alignment the WT and *nlp-40(tm4085)*, P1 to P4 indicates the predicted cleavage products of NLP-40, stars and dots indicate identity and similarity.

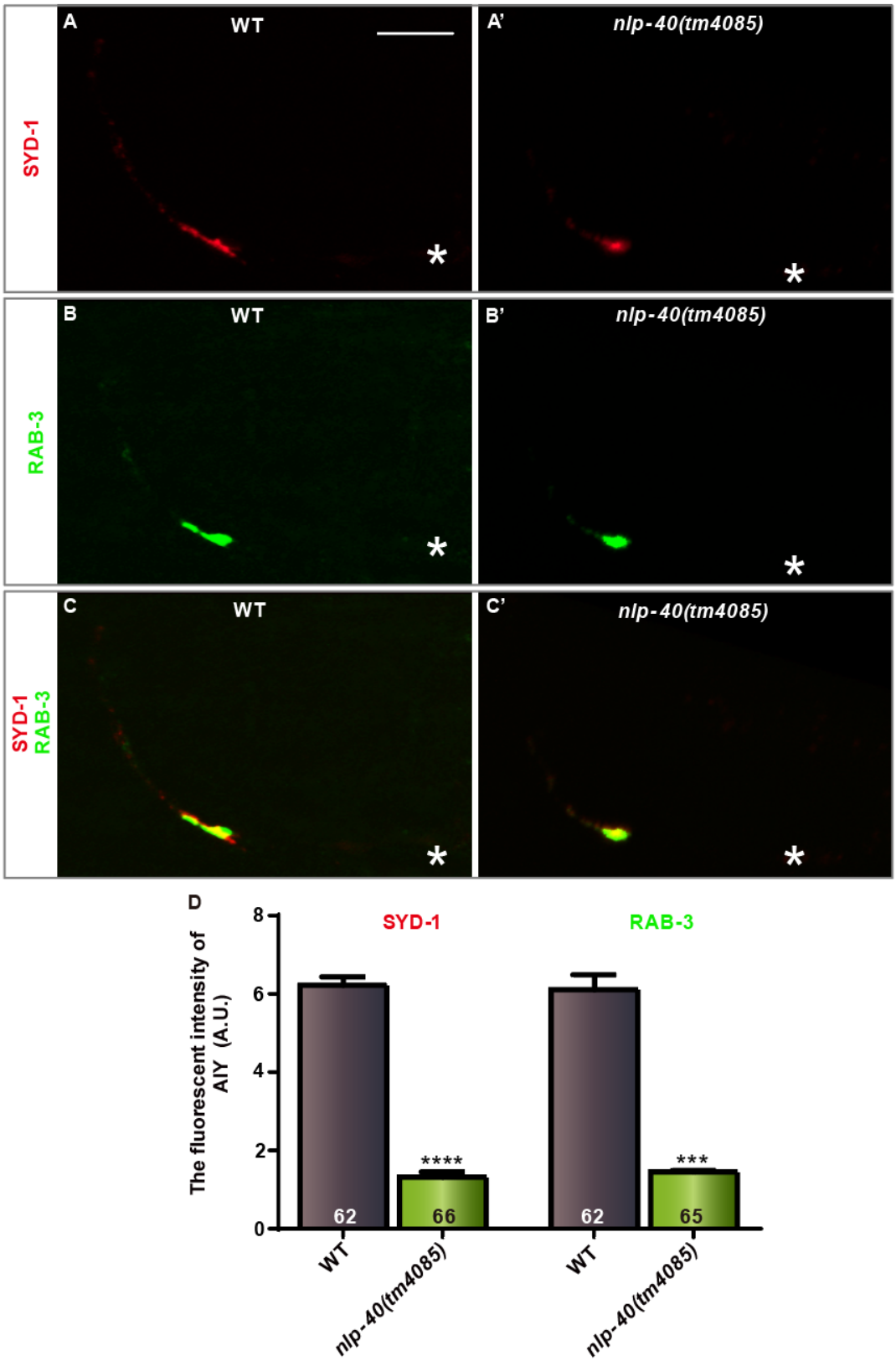

Supplementary Fig. 4 AIY presynaptic assembly requires *nlp-40*. (A-C') Confocal micrographs of the AIY synaptic active zone GFP::SYD-1 (pseudo-red) and synaptic vesicle marker mCherry::RAB-3 (pseudo-green) in wild type (A-B) and *nlp-40 (tm4085)* mutants (A'-B'). Those two presynaptic

markers are colocalized, as indicated in the merged images (C-C'). The scale bar in (A) is 10μm, applying to all image panels. (D) Quantification of the fluorescent intensity of AIY SYD-1 or RAB-3. Data are averaged from at least three biological replicates. The total number (N) of independent animals assayed is indicated in the bars. Statistical analyses are based on two-tailed Student's t-test. ***$p<0.001$, ****$p<0.0001$ as compared to WT. Error bars represent SEM.

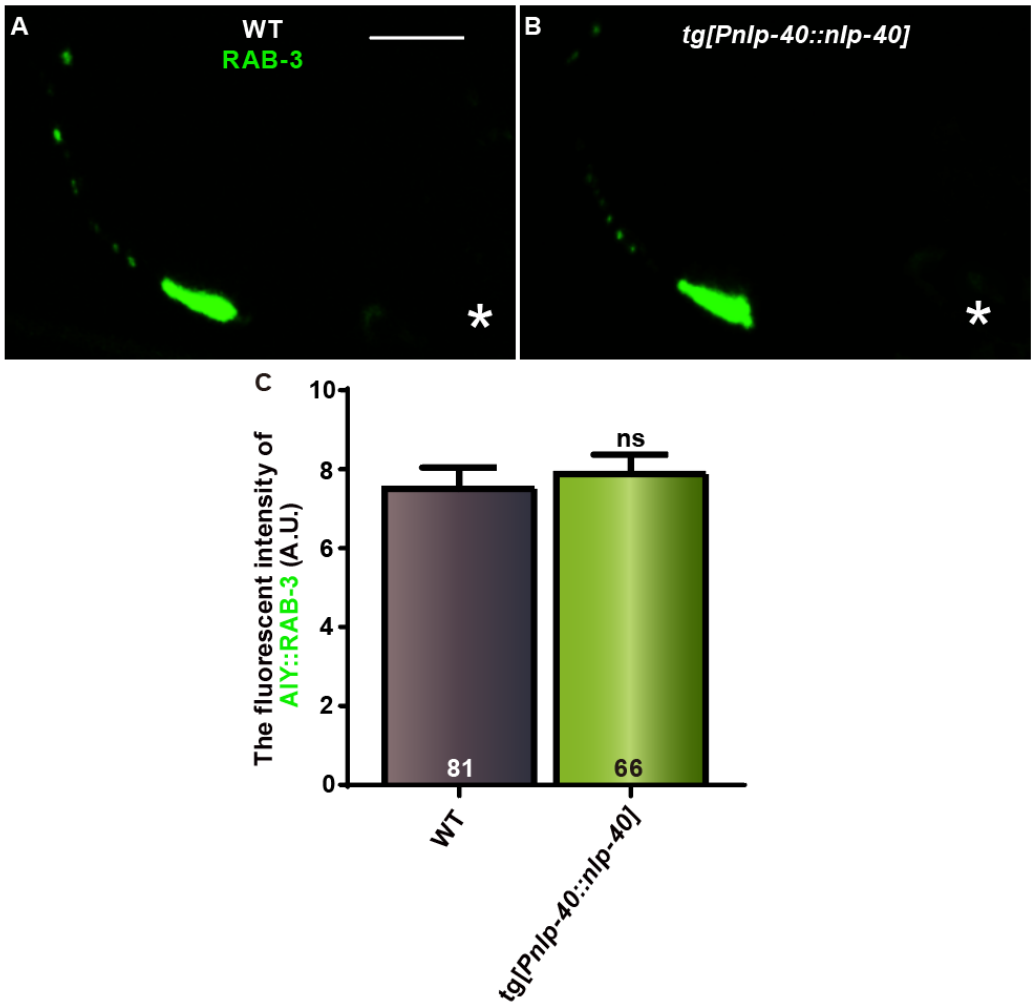

Supplementary Fig. 5 Overexpressing *nlp-40* is not sufficient to trigger AIY presynaptic assembly. (A-B) Confocal images of the AIY GFP::RAB-3 (A-B). The scale bar in (A) is 10μm, applying to (B). (C) Quantification of the fluorescent intensity of AIY RAB-3 for the indicated genotypes. Data for each genotype are averaged from at least three biological replicates. At least two independent lines were tested. The total number (N) of independent animals assayed is indicated in the bars. ns: not significant. Statistical analyses are based on two-tailed Student's t-test. Error bars represent SEM.

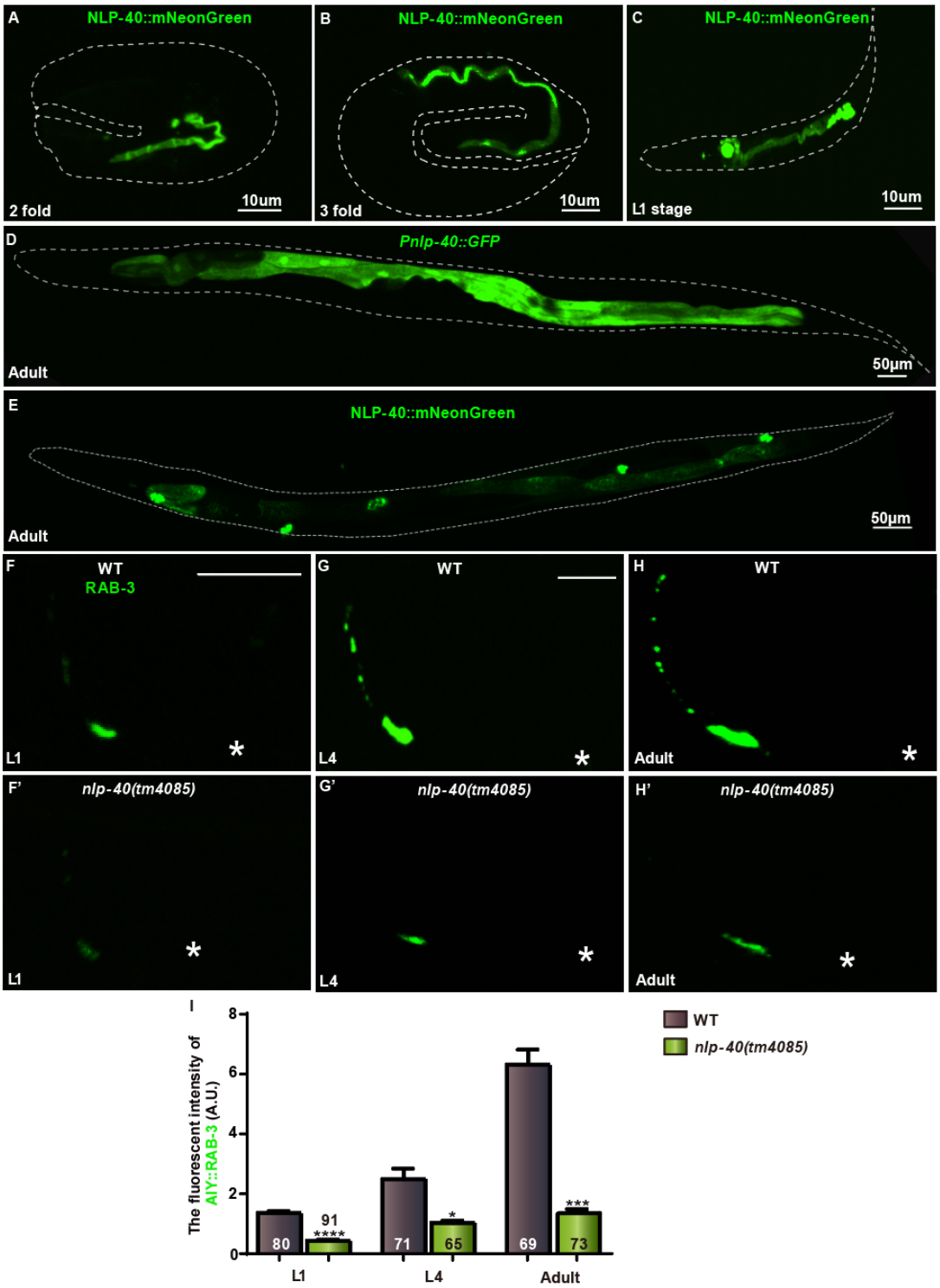

Supplementary Fig. 6 *nlp-40* is required for AIY synaptogenesis during embryonic and postembryonic development. (A-E) Confocal images of expression pattern and subcellular localization of embryonic stage, adult stage animals labeled with GFP or mNeonGreen respectively. Scale bars: 50μm.(F-H') Confocal micrographs of the AIY GFP::RAB-3 at L1 (F-F'), L4 (G-G') and adult day 1 (H-H') in wild type (F-H) and *nlp-40(tm4085)* mutant

(F'-H') animals. Asterisks indicate the AIY soma. The scale bar in (F) applies to (F'), and the one in (G) applies to (G', H and H'). Scale bars: 10μm. (I) Quantification of the fluorescent intensity of AIY RAB-3 for the indicated genotypes at the indicated stages. Data for each genotype are averaged from at least three biological replicates. The total number (N) of independent animals assayed is indicated in the bars. Statistical analyses are based on two-tailed Student's t-test. *$p < 0.05$, ***$p<0.001$, ****$p<0.0001$. Error bars represent SEM.

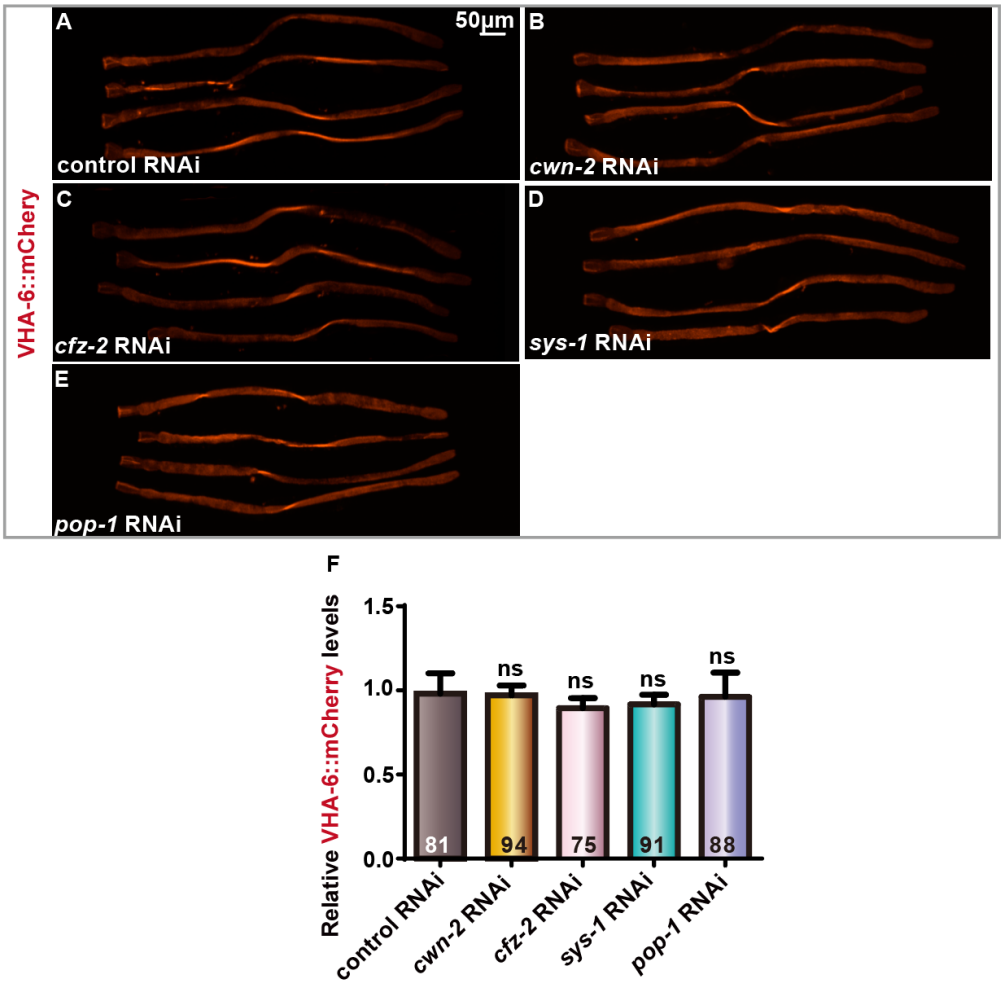

Supplementary Fig. 7 Wnts do not affect intestinal gene expression. (A-E) Confocal images of an intestinal-specific reporter VHA-6::mCherry in control (A), *cwn-2* (B), *cfz-2* (C), *sys-1* (D) and *pop-1* (E) RNAi animals at the adult day 1 stages. Scale bars: 50μm, applying for all images. (F) Quantification of VHA-6::mCherry fluorescent intensity for the indicated genotype. Data are averaged from at least three biological replicates. The total number (N) of independent animals assayed is indicated in the bars. Statistical analyses are based on one-way ANOVA followed by Dunnett's test. ns: not significant as compared to the control RNAi. Error bars represent 95% confidence interval.